Chapter 5

Investigation of Liquid-Phase Inhomogeneity on the Nanometer Scale Using Spin-Polarized Paramagnetic Probes

Valery F. Tarasov and Malcolm D.E. Forbes

Additional information is available at the end of the chapter

http://dx.doi.org/10.5772/67463

Abstract

The concept, basic physics, and experimental details of time-resolved electron paramagnetic resonance (TREPR) spectroscopy for the study of spin-correlated radical pairs (SCRPs) in heterogeneous media are presented and discussed. The delicate interplay between electron spin wave function evolution (governed by magnetic interactions such as the isotropic electron spin-spin exchange interaction and the electron-nuclear hyperfine interaction) and diffusion (governed by the size and microviscosity of the medium) provides a mechanism for assessing molecular mobility in confined spaces on the nanoscale (e.g., micelles, vesicles, and microemulsions). Experimental examples from micellar SCRPs are used to highlight the dominant features of the TREPR under different degrees of confinement and microviscosity, and spectral simulation methods are described to show how molecular mobility can be quantified.

Keywords: electron paramagnetic resonance, spin-correlated radical pairs, micelles, diffusion, microviscosity, confinement

1. Introduction

Electron paramagnetic resonance (EPR) spectroscopy is a fundamental method for the investigation of paramagnetic particles in liquid and solid solutions, in crystal and semiconductor substances, and in biological and physiological systems. Examples of such paramagnetic species include organic free radicals, transition metals such as Fe, Cu, Co, Ni, Mn, and their complexes, particularly dinitrosyl-iron complexes with thiol-containing ligands [1], excited molecular states (especially excited molecular triplets), quantum dots, and crystal defects. The EPR spectra of these systems provide valuable structural and dynamic information through spectral line shapes, g-factors, electron-nuclear hyperfine interactions, and electron spin relaxation processes. The electron and nuclear spin relaxation parameters depend on interactions

with their nearest paramagnetic neighbors and also on their molecular mobility. In this sense, all of the paramagnetic species mentioned above can be considered as useful probes of molecular motion and intermolecular interactions. However, extraction of the desired information from the EPR spectra can be time-consuming and this is not a simple computational task.

Nitroxide free radicals occupy an exceptional place among these species because they are minimally invasive and chemically stable. Their facile synthesis allows for the creation of a whole family of probes with different chemical structures and properties. Also, their EPR spectra are relatively simple, with only three resonant EPR transitions in most cases. The quantitative treatment of their spectra in isotropic media is based on a well-established and comprehensive theoretical analysis that is well documented in the literature [2–5]. For more complex situations involving the appearances of spectral anisotropies, or in the limit of slow motion, easily accessible and efficient computer programs have evolved for carrying out numerical simulations [6, 7] of the spectra. It is no surprise, therefore, that when the term "spin probe method" or "spin labeling" is used, it almost always refers first to the analysis of the EPR spectra of nitroxide radicals.

The nitroxide spin probe/label method has found wide applications in chemistry, biochemistry, and physics. Modern development of the method is deeply connected to recent advancements in EPR instrumentation. Examples include an increase in the microwave frequency [8, 9] up to 215–240 GHz (very high frequency EPR, VHF/EPR), application of pulsed EPR spectrometers [9, 10], as well as advances in targeted spin labeling (site-directed spin labeling, SDSL [11–13]). New chemical synthesis methods have resulted in novel probe structures designed, for example, to measure the polarity of the microenvironment surrounding the probe [14], the concentration of oxygen [15], and other properties in both homogeneous and heterogeneous systems.

There also exists a wide range of short-lived hydrocarbon radicals, typically transient species, that are observed as a result of photochemically or thermally initiated radical reactions. For some time, detectable EPR spectra of these intermediates were used only to verify or refute a particular mechanism of a chemical reaction [16, 17]. However, in 1963, Fessenden and Schuler reported highly unusual EPR spectra of hydrogen and deuterium atoms. Specifically, the low-field components of the hydrogen doublet and deuterium triplet were emissive, while the high-field components were absorptive [18]. These spectra were acquired at low temperatures during pulse radiolysis of liquid methane and deuteromethane. This spin-polarization phenomenon would have remained a curiosity, at the time attributed to an unexplained spin relaxation effect, if not for the discovery of the chemically induced dynamic nuclear polarization (CIDNP) a few years later. The CIDNP effect is defined as the creation of nonequilibrium populations of the nuclear spin states in the diamagnetic products of radical reactions involving recombination and disproportionation. The discovery of CIDNP in the 1960s [19, 20] stimulated deeper insights into the manifestations of the well-known rule of the electron spin-state conservation in chemical reactions, initially put forward by Wigner and Witmer [21]. By the end of the 1960s Closs, and independently, Kaptein and Oosterhoff, developed the so-called CKO model of CIDNP, which has been described in detail in several monographs (see for instance [22, 23]) and reviews [24–26]. This model allowed for a qualitative interpretation of all significant details of CIDNP but failed to provide much quantitative information. The main

drawback of the CKO model is an assumption of unrealistically long lifetimes for the radical pairs involved and a total disregard of the exchange spin-spin interaction between the unpaired electrons of the radical partners.

Consideration of the mutual diffusion of radicals as a continuum process under the modified Collins and Kimball boundary conditions [22, 27], or as Noyes diffusion flights (the so-called method of successive encounters [28]), removed these shortcomings and allowed researchers to formulate a model for liquid-phase spin-selective diffusion-controlled radical reactions—the radical pair mechanism (RPM) of CIDNP. In both the RPM and CKO models, the essence of CIDNP remains intact: it is based on the difference in the reactivity of singlet and triplet radical pairs.

The intensity of the spin-polarized NMR signal depends on the configuration of the nuclear spins in the radicals and on their coefficient of mutual diffusion. Therefore, at least in principle, the CIDNP magnitude could be used as a measurable parameter allowing for the extraction of information about the translation diffusion of radicals, for example, by comparing its value with the computed one. However, the RPM model is too idealized. The radicals are considered to be spherical particles, whose reactivity does not depend on orientation. The model operates in such terms as the thickness of a reaction layer in the reaction sphere or uses parameters in the Collins and Kimball boundary condition, the physical meanings of which are far from transparent. Additionally, it can operate in terms of distance-dependent reactivity of the radical pairs in the singlet electron spin state, with unknown or vague numerical values for the corresponding parameters. As a consequence, these circumstances make the quantitative conclusions about the molecular dynamics of radicals from the analysis of CIDNP data quite unreliable.

Contrary to CIDNP, the spin selectivity of radical recombination does not play such a crucial role in the generation of CIDEP. Nevertheless, nuclear spin-dependent singlet-triplet mixing is still a necessary step for the observation of CIDEP via the RPM. However, instead of a reaction taking place from a specific electron spin state, the relative phase shifts of the electron spin singlet and triplet states induced by the distance-dependent electron spin exchange interaction become a crucial factor for the development of CIDEP [29, 30]. Not all such repetitive encounters are efficient in the creation of CIDEP. The pair must not spend too long time at distances where the spin's exchange interaction is zero. Also, this time must be comparable with the difference in the Larmor frequencies of the radicals. On the other hand, the lifetime of the contact pairs must not be too short, that is, there should be enough time for efficient dephasing between the multiplicative electron spin states of a pair. Therefore, CIDEP created by the RPM, ST_0RPM in the particular case of the high-field approximation, is observed in radicals that became involved in secondary encounters after rather long (several tens of Å) diffusional journeys [29–34].

As in the case of other mechanisms of CIDEP such as the triplet mechanism (TM) [34], the electron spin polarization transfer (ESPT) [35, 36], and the radical triplet pair mechanism (RTPM) [37], the observed EPR signals, usually acquired in a time-resolved experiment, belong to “free” radicals and are characterized by the same line widths and resonance frequencies as if the radicals were in the Boltzmann equilibrium state (nonpolarized). But the molecular mobility

information potentially extractable from these parameters can be obtained using the nitroxide spin probe method in a more efficient and less expensive way. On the other hand, the polarization patterns observed in TREPR experiments carry additional information about the interaction of radicals with each other. Due to the length of the diffusional trajectories, this information is much less local and therefore may be of significance to researchers working in heterogeneous media on the nanoscale (micelles, vesicles, and microemulsions).

This unique property of CIDEP via the RPM is manifested most clearly when the diffusion of the radicals is limited by a physical boundary, so that all the diffusional trajectories of the radical pair satisfy the conditions listed above. Under such conditions, each individual spectroscopic line in each radical's TREPR spectrum is split into two lines of opposite phase and gives rise to what Shushin [38], in 1991, dubbed as the "Anti-Phase Splitting," (APS). The corresponding model of CIDEP for such cases is called the spin-correlated radical pair mechanism or SCRPM [39]. In this chapter, we will revisit several systems involving radical pair confinement with restricted diffusion in the context of some unusual experimental observations. Our goal is to show that SCRPs are very valuable spin probes for self-organizing molecular systems such as micelles, vesicles, microemulsions, and potentially for any medium with the characteristic sizes of inhomogeneity on the nanometer scale.

2. Features of TREPR spectroscopy: spin-polarized "free" radicals

The TREPR technique uses continuous wave (cw) microwave excitation in the same way as commercial steady-state EPR (SSEPR) spectrometers: The TREPR transitions are detected by sweeping an external magnetic field B through each resonance at a constant microwave frequency ω_0. The TREPR operates in so-called direct detection mode (**Figure 1**) in the sense that the 100-KHz field modulation normally employed in SSEPR is disabled. **Figure 1** shows

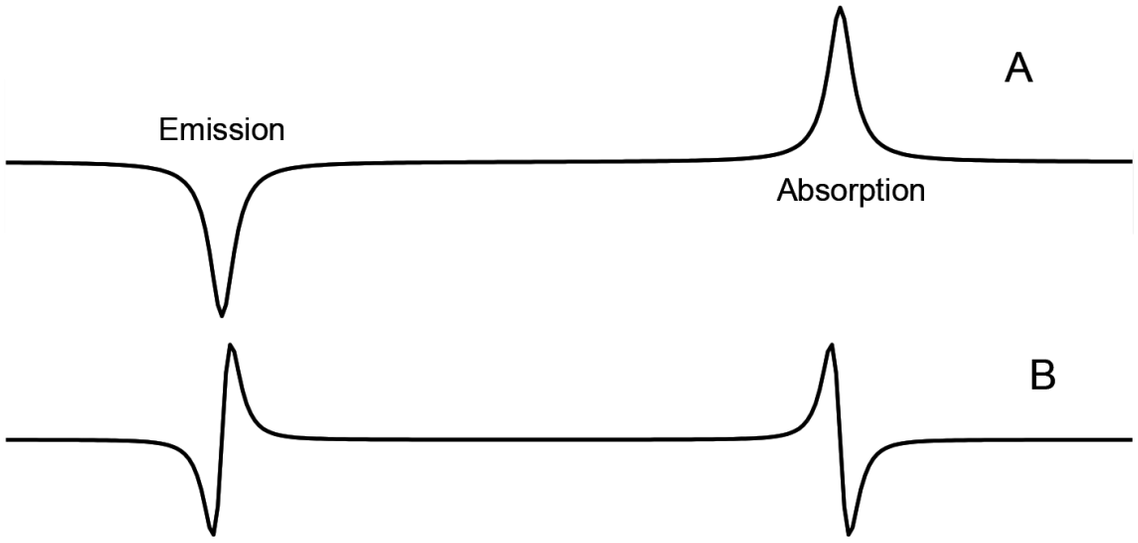

Figure 1. (A) EPR doublet signal acquired in "direct detection" mode (TREPR). (B) The same signal acquired with magnetic field modulation (SSEPR). Note that the first derivative lines in trace B have opposite phases.

http://dx.doi.org/10.5772/67463

the comparison of an EPR signal acquired in the "direct detection" mode (trace A, TREPR) with a signal from the same radical species detected with field modulation (trace B, SSEPR). Trace B, which shows the first derivative line shape, is exactly the signal observed by Fessenden and Schuller [18] in their discovery of electron spin polarization. Note the opposite phases of the low- and high-field transitions in both traces.

Detection of TREPR signals in the direct detection mode results in a significant loss in sensitivity compared to SSEPR. But this shortcoming is compensated efficiently by the gain in time response, since the TREPR signal is coming directly from the spectrometer's microwave bridge preamplifier circuit and is sampled electronically on a short timescale after its creation. The time response at X-band is generally limited by the resonator quality factor to about 50 ns. Higher-frequency W-band spectrometers (95 GHz) allow for much higher time resolution (down to 2.5 ns) [37]. Unfortunately, technical problems, such as delivering light to the sample and the difficulty of using flow systems, significantly narrow the applicability of W-band spectrometers.

The Lorentzian line shape of the resonance signals in SSESR experiments is ensured in liquid solutions via the steady state Bloch equations, that is, under conditions of the absence of saturation, the time interval between the creation of magnetization and its detection t_{obs} should be much longer than the relaxation time T_2 or $t_{obs}/T_2 \gg 1$. Typical transverse relaxation times of organic radicals range from tens of nanoseconds to several microseconds. This means that in many cases, the condition $t_{obs}/T_2 \gg 1$ is unfulfilled. It is worthwhile to consider in this case, what happens to the resonance line shape.

Figure 2 shows TREPR spectra of geminate radical pairs (**Scheme 1**) resulting from photo-induced Norrish type-I cleavage (Nd-YAG, $\lambda = 355$ nm) of 2,2-dimethoxy-1,2-diphenyl ethane-1-one (trade name: Irgacure®651) in aqueous SDS micellar solutions at room temperature [40, 41]. The TREPR spectra in **Figure 2** were acquired at the outlet of a microwave bridge-wide bandwidth preamplifier (12 MHz gate), using a LeCroy digital oscilloscope at $t_{obs} = 260$ ns (A), $= 1.12$ μs (B), and $= 3.6$ μs (C)

The spectra in **Figure 2** are strongly polarized by the TM. The most striking feature of the spectra is the strong dependence of the width of the spectral lines on the observation time t_{obs}. The line width at the longest observation time $t_{obs} = 3.6$ μs (trace C) corresponds to $T_2 = 1.2$ μs for the $\alpha\alpha$-dimethoxybenzyl radical. The condition $t_{obs}/T_2 \gg 1$ is not, strictly speaking, fulfilled even for $t_{obs} = 3.6$ μs and far from being fulfilled for the other two cases: $t_{obs} = 260$ ns and $t_{obs} = 1.12$ μs. Thus, one can suggest that the additional line broadening is either caused by modulation of the inter-radical electron spin interactions due to the molecular diffusional motion of radicals or some inherent properties of the EPR spectra observed under conditions of the violation of the inequality $t_{obs}/T_2 \gg 1$ or both. At the moment, we do not need a detailed discussion of this problem; it will be quite enough to show how the resonance line appears in the TREPR experiment at $t_{obs}/T_2 \leq 1$. A similar analysis has been performed already using a set of modified Bloch equations [42, 43].

In a frame rotating with the angular velocity ω_0 around the direction of the magnetic field of spectrometer B, the spin and its interaction with the resonance microwave field are represented

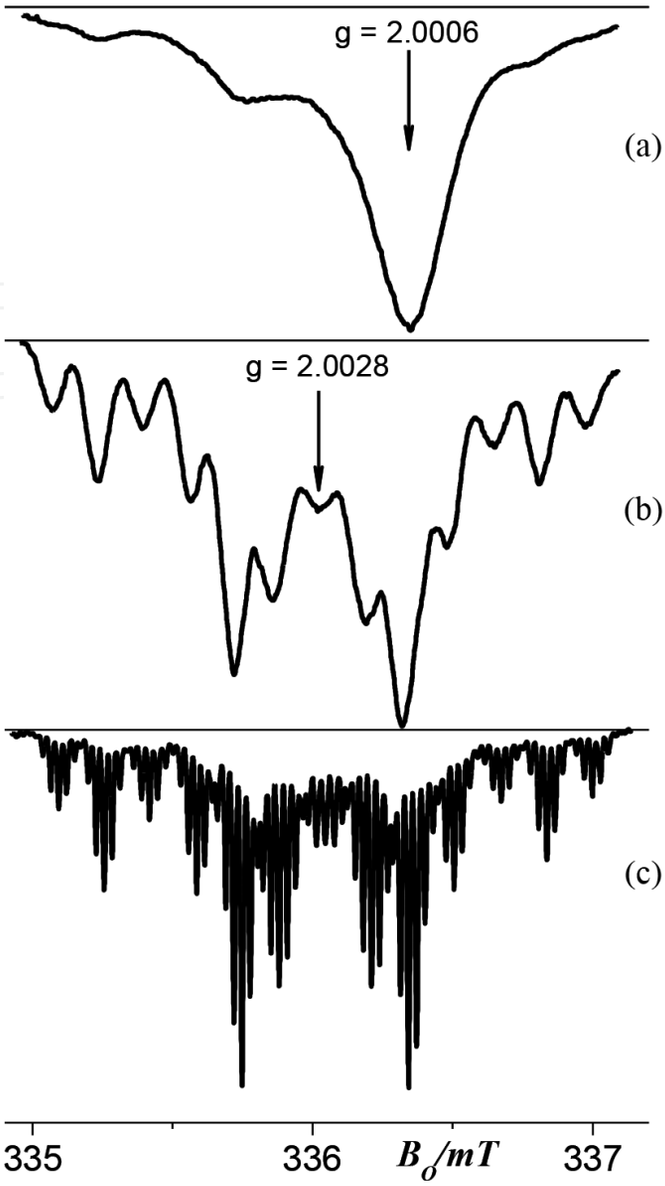

Figure 2. TREPR spectra at t_{obs} = 260 ns (a), = 1.12 μs (b), and = 3.6 μs (c) of geminate radical pairs resulting from photodissociation of Irgacure®651 (**Scheme 1**) in micellar aqueous solutions of SDS at room temperature [40, 41].

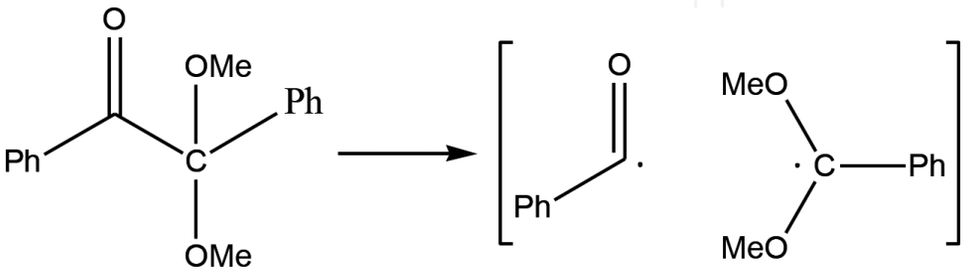

Scheme 1. Photoexcitation (355 nm) of 2,2-dimethoxy-1,2-diphenyl ethane-1-one (Irgacure®651) resulting in Norrish type-I cleavage. This reaction is very fast and forms a geminate triplet pair of benzoyl (g = 2.0006) and $\alpha\alpha$-dimethoxybenzyl (g = 2.0028) radicals.

http://dx.doi.org/10.5772/67463

by the time-independent spin operators $\hat{H}$ and $\hat{H}_{\mu w}$ respectively. Then, the corresponding Liouville equation (LE) for the spin-state vector **ρ** reads:

$$\frac{d\boldsymbol{\rho}}{dt} = \{-i(\hat{\hat{H}} + \hat{\hat{H}}_{\mu w}) + \hat{\hat{R}}\} \cdot \boldsymbol{\rho} \tag{1}$$

Super operators $\hat{\hat{H}}$ and $\hat{\hat{H}}_{\mu w}$ in the Liouville spin space are associated with the commutators in the Hilbert spin space $[\hat{H}, \hat{\rho}] \Rightarrow \hat{\hat{H}} \cdot \boldsymbol{\rho}$, $[\hat{H}_{\mu w}, \hat{\rho}] \Rightarrow \hat{\hat{H}}_{\mu w} \cdot \boldsymbol{\rho}$, respectively, and the state vector **ρ** is comprised of elements of the spin density operator $\hat{\rho}$. $\hat{\hat{R}}$ is the relaxation super operator.

This situation is commonly encountered when the particular mechanism of paramagnetic relaxation is unknown or when several mechanisms operate simultaneously. In our work, we use the phenomenological relaxation superoperator—the matrix representation of which in the eigenbasis of $\hat{H}$ and in the high-field approximation limit is given by Eq. (2):

$$\hat{\hat{R}} = \begin{pmatrix} -k_1 e^{\beta} & 0 & 0 & k_1 e^{-\beta} \\ 0 & -k_2 & 0 & 0 \\ 0 & 0 & -k_2 & 0 \\ k_1 e^{\beta} & 0 & 0 & -k_1 e^{-\beta} \end{pmatrix} \tag{2}$$

where $k_1 = 1/2T_1$ is assumed to be the same for all pairs of the electron-nuclear spin levels. We also suggest that all the off-diagonal elements of the density matrix decay with the same rate constant $k_2 = 1/T_2$. The relaxation super operator (2) ensures the Boltzmann equilibrium of the spin ½ at $t \to \infty$ if k_2 and k_1 are real and positive. Since we solve Eq. (1) in rotating frame of reference, then it is quite natural to wonder why do we do believe that in the rotating frame the spin ensemble relaxes to the **B** direction instead of the effective magnetic field in the rotating frame. See Redfield [44] for the discussion of this problem.

Eqs. (1)–(2) are applicable to any time of observation (t_{obs}) and lead to a Lorentzian shape, Eq. (3), of the resonance line if $t_{obs} \gg T_2$ and $\omega_1 << (T_1, T_2)^{-1/2}$,

$$I(\omega) = \frac{1}{\pi} \frac{T_2^{-1}}{T_2^{-2} + (\omega - \omega_r - \Delta_r)^2} = \frac{T_2}{\pi} \frac{1}{1 + (\omega - \omega_r - \Delta_r)^2 T_2^2} \tag{3}$$

where ω_r and Δ_r are the resonance frequency and the spectral shift induced by relaxation, respectively.

Figure 3 shows the TREPR spectra of an electron spin ½ being initially in the spin state $|\beta\rangle$ or $\hat{\rho_0} = \begin{pmatrix} 0 & 0 \\ 0 & 1 \end{pmatrix}$. For all calculations, $B_1 = 0.01$ G, $T_1 = 5$ μs, $T_2 = 0.25$ μs (**Figure 3A** and **3B**), and 80 ns (**Figure 3C** and **3D**). $t_{obs} = 0.2$ μs (A, B and C), and $t_{obs} = 25$ μs (Boltzmann population, Trace D). Traces A and C in **Figure 3** demonstrate what happens when the *cw* TREPR spectra are acquired at such t_{obs} that the inequality $t_{obs}/T_2 \gg 1$ is not fulfilled. Side wiggles cause an extra broadening [43] of the resonance lines. Comparing the A and C spectra in **Figure 3** suggests that when t_{obs} is comparable with T_2, the width of the resonance line is defined

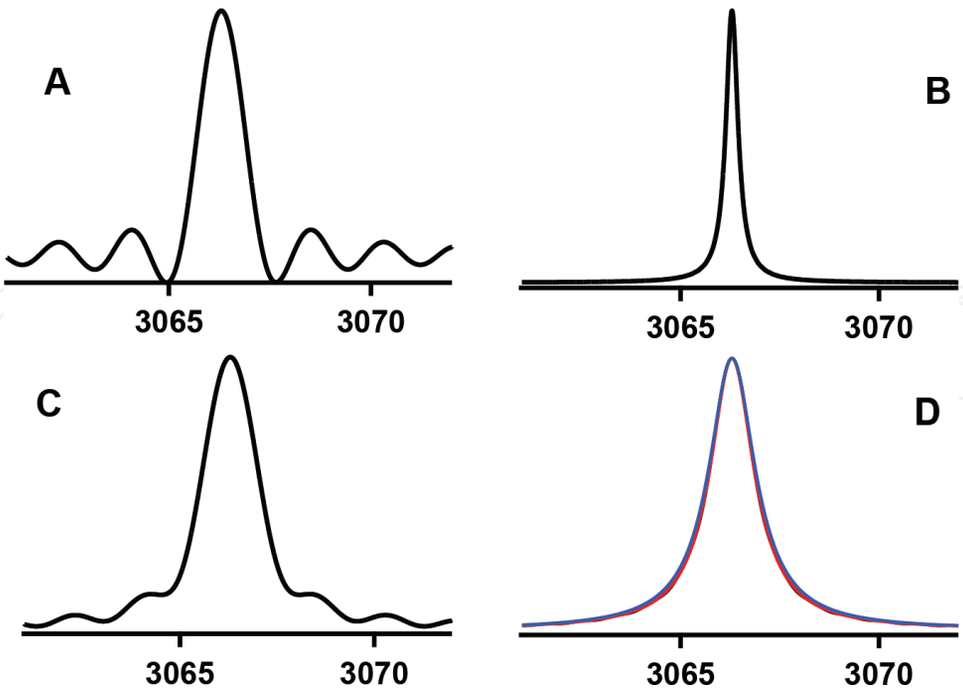

Figure 3. Calculated TREPR spectra using Eqs. 1, 2 for $B_1 = 0.01$ G and $T_1 = 5$ μs. Trace A: t_{obs} (= 0.2 μs)/T_2 (= 0.25 μs) = 0.8; Trace B: t_{obs} (= 2 μs)/T_2 (= 0.25 μs) = 8; Trace C: t_{obs} (= 0.2 μs)/T_2 (= 0.08 μs) = 2.5; Trace D (Boltzmann equilibrium): t_{obs} (= 25.6 μs)/T_2 (= 0.08 μs) = 320.

practically entirely by t_{obs} and does not depend on the transversal relaxation time T_2. A comparison of traces B and D in **Figure 3** shows that shorter the relaxation time T_2, the longer the time interval when the shape of the resonance line does not depend on t_{obs}. For instance, at $T_2 = 80$ ns, the shape of the resonance line only slightly differs from that for a radical at Boltzmann equilibrium (trace D), even at $t_{obs} = 400$ ns.

3. The SCRP mechanism and its manifestation in the TREPR spectra

In the previous paragraph, we have shown that the width of the EPR resonance line, a key parameter of the SSEPR spin probe method, is not suitable for the TREPR spin-polarized method because it depends on t_{obs}. Even when it would seem that the line width does not depend upon t_{obs}, it still remains an unreliable measurable parameter, because the shape of the TREPR resonance line is slightly different from Lorentzian, appearing slightly narrower than what would be observed for the same radical resonance line at Boltzmann equilibrium (**Figure 3D**). The polarization patterns inherent to such mechanisms of CIDEP, as ESPT, RTPM, and RPM contain very valuable information concerning the multiplicity of radical pairs, or radical–triplet pairs, the distribution of electron–nuclear spin populations in the excited spin-not-equilibrated triplet, or the signs of the exchange interactions. However, this is mostly information about the radical pair itself. Extraction of information about molecular motion from these experiments, that is, using the polarization patterns of free radicals observed in TREPR experiments, and their time evolution, is accompanied by many theoretical and

http://dx.doi.org/10.5772/67463

computational difficulties, see for instance [42, 43, 45, 46]. This has motivated us to obtain further insight into the analysis of the CIDEP patterns of radical pairs experiencing restricted translation diffusion.

3.1. History: the quasi-static approximation (QSA)

For the better part of the past three decades, SCRPs have been a topic of keen interest in the field known as "spin chemistry." Many structurally distinct types of SCRPs have been studied by the TREPR [47–50] and NMR [51–53] spectroscopy, including resonance microwave field effects on nuclear spin polarization [54], on chemical product reaction yields [55–60], and on internal magnetic field effects [61, 62]. It is important to note that SCRPs represent a true case of entangled spin states. For this reason, SCRPs find themselves at the forefront of quantum computing research [63–66] and of high relevance to the more general field of spintronics [67].

In the EPR spectroscopy community, the term "SCRP" was put into use in 1987 by Buckley et al. [68]. The necessity of a specific term was justified by the observation of specific line shapes in the TREPR spectra resulting from photochemical reactions of acetone with isopropanol in liquid solutions: each resonance line of the acetone ketyl radical was split into two oppositely polarized components exhibiting an emission/absorption (E/A) pattern. In 1989, the nomenclature for this spectral pattern was abbreviated by Shushin [38] as the APS. It is worthwhile to note that there were a few earlier publications [69–72] that reported APS-like spectral patterns, but these reports either suggested no interpretation or interpretations that were unlikely to be correct.

An example of the APS feature in a TREPR spectrum is given in **Figure 4**, where spectrum A belongs to a radical pair (**Scheme 2**) generated by the laser flash photolysis of ^{13}C-labeled in the carbonyl group 2,2-dimethyl-desoxy-benzoin (DMDB) in an aqueous micellar solution of SDS at room temperature.

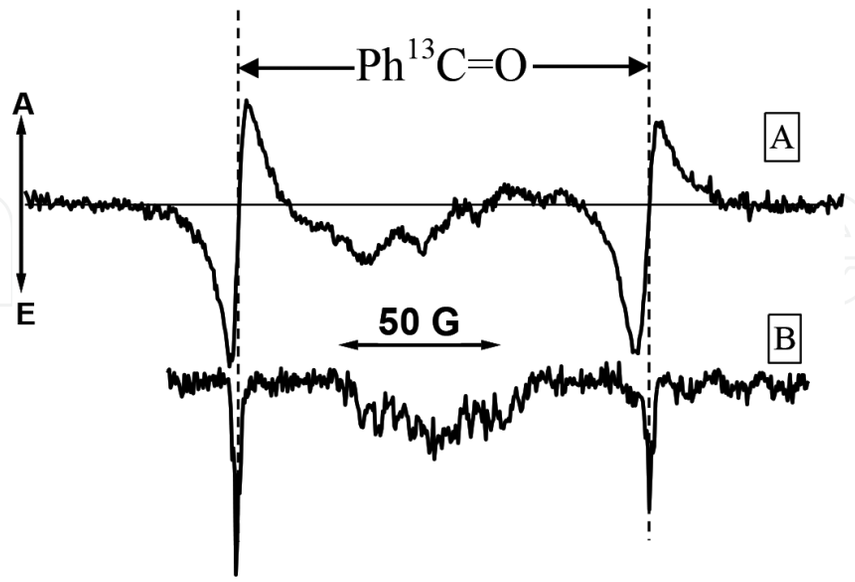

Figure 4. The TREPR spectra of radical pairs comprised of ^{13}C-benzoyl and cumyl radicals resulting from the photochemical reaction shown in **Scheme 2** via laser photolysis flash (λ = 308 nm) at room temperature in (A) aqueous SDS micellar solutions and (B) in viscous ethanol:cyclohexanol = 1:4 mixture. In both spectra, t_{obs} = 360 ns.

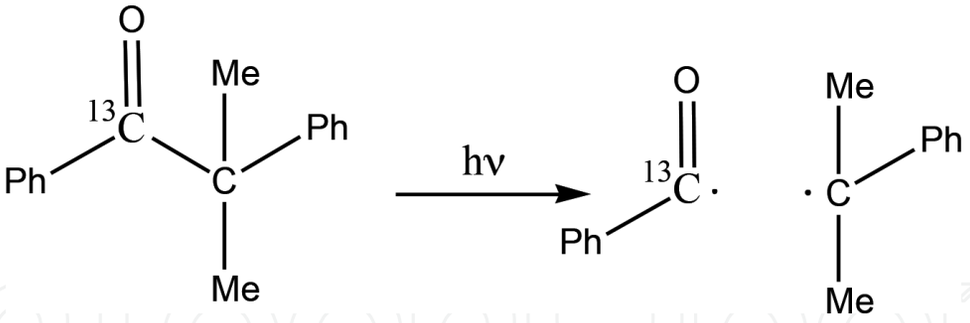

Scheme 2. Photoexcitation ($\lambda = 308$ nm) of 2,2-dimethyl-1,2-diphenylethane-1-[^{13}C] on (DMDB) resulting in a geminate triplet radical pair consisting of [^{13}C]benzoyl ($g = 20006$) and cumyl ($g = 2.0028$) radicals. See Ref. [67] for details.

Spectrum B in **Figure 4** belongs to the same radical pair acquired at the same $t_{obs} = 360$ ns and under the same experimental conditions (temperature, microwave power, etc.) except that spectrum B was obtained for laser photolysis in a homogeneous mixture of solvents ethanol: cyclohexanol = 1:4, which has a similar viscosity to that in the SDS micellar core. Spectra A and B in **Figure 4** are both composed of doublets from the ^{13}C-benzoyl radical and multiplet signals in the center from the cumyl radical. Each component of the benzoyl doublet is E/A split in **Figure 4A**, while in **Figure 4B**, the same doublet is TM polarized and does not contain any additional splitting. The spectrum of the cumyl radical shows the same difference in spectral features between micelles and free solution, although not quite so evidently due to the complexity of the spectrum.

Another example of a TREPR spectrum exhibiting the APS is shown in **Figure 5**. As before, the spectra in traces A and B arise from the same radical pair (**Scheme 3**) with only one difference: while trace A belongs to the radical pair generated by photoreduction of benzophenone in SDS micelles, that is, located inside the micellar phase, trace B represents the same radical pair observed in liquid solution, where they move freely. The CIDEP of the radicals in trace B is

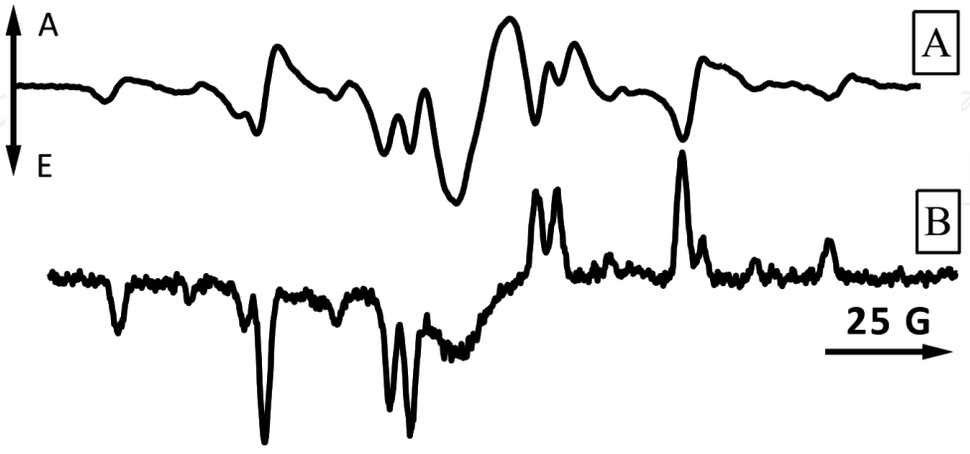

Figure 5. TREPR ($t_{obs} = 500$ ns) spectra of geminate pairs Alk· and BPH· radicals produced in photochemical ($\lambda = 308$ nm) oxidation of SDS detergent by the electronically excited triplet state of benzophenone (0.4 mM) in micellar aqueous solution of SDS (10 mM) (A) and benzophenone (0.4 mM) in ACN/H2O = 50:50 solution of SDS which does not contain micelles.

http://dx.doi.org/10.5772/67463

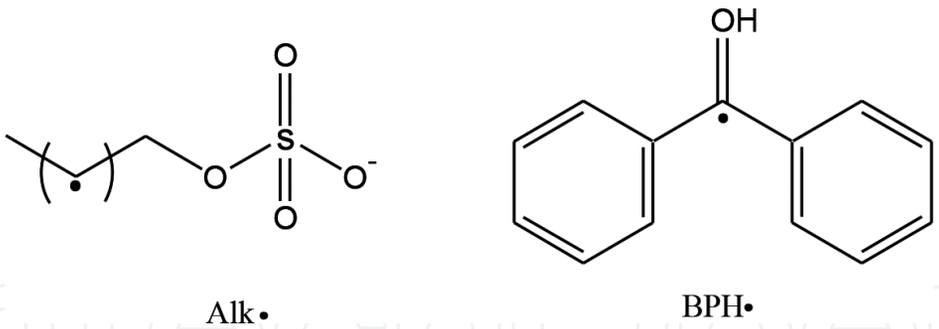

Scheme 3. Chemical structure of Alk· and BPH· radicals produced in the photochemical oxidation of SDS detergent by the electronically excited triplet state of benzophenone.

mostly due to the RPM. There is a noticeable contribution from the TM polarization, but there is no APS. Neither the TM nor the RPM polarization patterns are observed in trace A, where diffusion is restricted. The results presented in **Figures 4** and **5** are intriguing as they represent a measurable physical change that is imposed only by a boundary condition on radical diffusion. This suggests that SCRPs might be used as "polarized spin probes" to investigate molecular and spin dynamics in inhomogeneous media, even in a qualitative fashion, that is, as a method of sensing restricted mobility.

Important and pioneering theoretical work by Buckley et al. [68], Closs et al. [73] was brought forward in the 1980s to explain the APS phenomenon, and it was based on two central ideas:

1. In a chemical reaction resulting in a geminate radical pair, the population of the SCRP electron-nuclear spin states proceeds so quickly that the electron spin state of the precursor remains intact, irrespective of the magnitude of any inter-radical spin-spin interactions operating during the process of radical pair creation.

2. The presence of inter-radical electron spin exchange and dipolar magnetic interactions leaves an inherent double degeneracy of the EPR transitions in a pair of magnetically non-equivalent electron spins, resulting in an additional splitting of the EPR spectral lines similar to that what is going on in the SSEPR spectroscopy of stable nitroxide biradicals [74].

But despite the full consent in the two fundamental principles, understanding how this inter-radical interaction is manifested in the TREPR spectroscopy is completely different.

According to [68], the spectrum consists of contributions from immobilized SCRPs, with the radical partners diffused apart and separated by whatever inter-radical distances $r(t_{obs})$ have been attained at the moment of observation t_{obs}. The inter-radical electron spin exchange interaction depends on these distances and consequently on t_{obs}, that is, $J_{ex} = J\left(r(t_{obs})\right)$. It follows that the instantaneous Hamiltonian of a radical pair $H(\hat{t_{obs}})$, and its resonant magnetic fields $\omega_i(t_{obs})$ will also depend on t_{obs}. From this, we conclude that the overall spectrum was calculated as purely inhomogeneous. All possible TREPR transitions, corresponding to each instantaneous Hamiltonian, are assumed to possess the same T_2, which becomes a parameter to be varied to best fit. The intensities of the EPR resonance lines were believed to be

proportional to the product of the difference in populations of corresponding electron spin eigenstates of the instantaneous Hamiltonian times the probability of the EPR transition. This is the origin of what we call the *quasi-static approximation* or QSA.

There are rather obvious disadvantages of the QSA. First, it cannot account for the generation of CIDEP due to the RPM (both ST_0 and $ST_{\pm}$), which strongly contradicts experimental observations (see **Figures 4B** and **5B**). Instead, one has to take this polarization pattern into account artificially (see **Figure 3** in Ref. [68]). Second, the TREPR spectrum at t_{obs} for the instantaneous $H(\hat{t_{obs}})$ would be a single resonance line with a particular T_2 (see Section 1 of the chapter) only if the instantaneous Hamiltonian evolved adiabatically (in the sense of energy levels) or nonadiabatically (in the sense of spin quantum numbers). In other words, a pair of acetone ketyl radicals would have to diffuse so slowly that they remained at distances r (t_{obs}), where the exchange interaction is comparable to the hyperfine interaction, for at least such a time t_r that $t_r > T_2$, which may not be realistic. Third, T_2 cannot be considered as an independent parameter because modulation of the inter-radical electron spin interactions can be the main reason for spectral line broadening (T_2). For example, see **Figures 4A** and **5A**, where the components of the APS are much broader than those in **Figures 4B** and **5B**.

The instantaneous spin Hamiltonian $\hat{H}(J)$ of a pair of radicals ***a*** and ***b*** in the high-field approximation can be written as the sum:

$$\hat{H}(J) = \hat{h}_a + \hat{h}_b + \hat{J}_{ex} \tag{4}$$

where

$$\hat{J}_{ex} = -J_0 \cdot \left(\frac{1}{2} + 2\hat{\mathbf{S}}_a \cdot \hat{\mathbf{S}}_b\right) \cdot \exp\left(-\frac{r-R}{\lambda}\right) \tag{5}$$

describes the instantaneous inter-radical electron spin-spin Heisenberg exchange interaction, R is the radius of the contact sphere (the distance of closest approach for the case of spherical radicals), J_0 is the exchange interaction at R, and the spin Hamiltonians of separated radicals $\hat{h_a}$ and $\hat{h_b}$ are given by Eq. (6).

$$\hat{h}_a = \frac{1}{2} \cdot \begin{pmatrix} \omega_a & 0 \\ 0 & -\omega_a \end{pmatrix} \otimes \begin{pmatrix} 1 & 0 \\ 0 & 1 \end{pmatrix}; \; \hat{h}_b = \begin{pmatrix} 1 & 0 \\ 0 & 1 \end{pmatrix} \otimes \frac{1}{2} \cdot \begin{pmatrix} \omega_b & 0 \\ 0 & -\omega_b \end{pmatrix} \tag{6}$$

ω_a and ω_b are the Zeeman frequencies of the electron spins in the magnetic field of the spectrometer and for a particular configuration of the magnetic nuclei $\{\chi\} = \{\chi_a\} \otimes \{\chi_b\}$ in SCRP which is defined by nuclear spin configurations $\{\chi_a\}$ and $\{\chi_b\}$ in radicals. The eigenvalues and eigenfunctions in the multiplicative electron spin basis

$$|\alpha\alpha;\chi\rangle, \; |\alpha\beta;\chi\rangle, \; |\beta\alpha;\chi\rangle, \; |\beta\beta;\chi\rangle \tag{7}$$

of the spin Hamiltonian (4) are given in **Table 1**. If $2q > 0$ and $J < 0$, the electron spin states at $-J \gg q$ (contact pair) and at $J = 0$ (separate pair) correlate as shown in **Figure 6**. When $J \neq 0$ two twice degenerated EPR transitions in the system of two non-interacted ($J = 0$) radicals ***a*** and b $|\psi_1\rangle \leftrightarrow |\psi_3\rangle = |\alpha\alpha\rangle \leftrightarrow |\beta\alpha\rangle$; $\quad |\psi_4\rangle \leftrightarrow |\psi_2\rangle = |\beta\beta\rangle \leftrightarrow |\alpha\beta\rangle$ $\quad$ and $\quad |\psi_1\rangle \leftrightarrow |\psi_2\rangle = |\alpha\alpha\rangle \leftrightarrow |\alpha\beta\rangle$;

Eigenvalues	Eigenfunctions	$-J \to 0$	$-J \to \infty$	
$\omega - J$	$\lvert\psi_1\rangle = \lvert\alpha\alpha\rangle$	$\lvert\alpha\alpha\rangle$	$\lvert\alpha\alpha\rangle$	(8a)
ε	$\lvert\psi_2\rangle = \cos(\theta/2)\lvert\alpha\beta\rangle + \sin(\theta/2)\lvert\beta\alpha\rangle$	$\lvert\alpha\beta\rangle$	$\frac{1}{\sqrt{2}}(\lvert\alpha\beta\rangle + \lvert\beta\alpha\rangle)$	(8b)
$-\varepsilon$	$\lvert\psi_3\rangle = -\sin(\theta/2)\lvert\alpha\beta\rangle + \cos(\theta/2)\lvert\beta\alpha\rangle$	$\lvert\beta\alpha\rangle$	$\frac{1}{\sqrt{2}}(-\lvert\alpha\beta\rangle + \lvert\beta\alpha\rangle)$	(8c)
$-\omega - J$	$\lvert\psi_4\rangle = \lvert\beta\beta\rangle$	$\lvert\beta\beta\rangle$	$\lvert\beta\beta\rangle$	(8d)
where $\omega = \frac{1}{2}(\omega_a + \omega_b)$; $q = \frac{1}{2}(\omega_a - \omega_b)$; $\varepsilon = \sqrt{q^2 + J^2}$; $\cos(\theta) = \frac{q}{\varepsilon}$; and $\sin(\theta) = -\frac{J}{\varepsilon}$				(9)

Table 1. Eigenfunctions and eigenvalues of the spin Hamiltonian Eqs. (4)–(6).

$|\psi_4\rangle \leftrightarrow |\psi_3\rangle = |\beta\beta\rangle \leftrightarrow |\beta\alpha\rangle$ convert into four distinguished EPR transitions shown in the bottom of **Figure 6**.

In **Figure 6**, the EPR transitions $|\psi_1\rangle \leftrightarrow |\psi_2\rangle$, $|\psi_2\rangle \leftrightarrow |\psi_4\rangle$ are labeled as *T*-type transitions because the pair spin state $|\psi_2\rangle$ correlates with the triplet $\frac{1}{\sqrt{2}}(|\alpha\beta\rangle + |\beta\alpha\rangle) = |T_0\rangle$ spin state when $-J \to \infty$. Correspondingly, the transitions $|\psi_1\rangle \leftrightarrow |\psi_3\rangle$ and $|\psi_3\rangle \leftrightarrow |\psi_4\rangle$ are labeled as *S*-type transitions. When $|J| \ll |q|$ the spin transitions $|\psi_1\rangle \leftrightarrow |\psi_3\rangle$ and $|\psi_2\rangle \leftrightarrow |\psi_4\rangle$ represent resonant flips of spin **a;** therefore, these transitions are labeled as the *a*-type transitions T_a and S_a. Similarly, $|\psi_1\rangle \leftrightarrow |\psi_2\rangle$ and $|\psi_3\rangle \leftrightarrow |\psi_4\rangle$ spin transitions are called *b*-type transitions T_b and S_b. The labels T_a, T_b, S_a, and S_b will be used throughout this work. In the case of the triplet precursor and absence of the TM polarization, all the three spin states $|T_0;\chi\rangle$ and $|T_\pm;\chi\rangle$ are populated equally: $\rho_{T_+T_+} = \rho_{T_0T_0} = \rho_{T_-T_-} = 1/3$. Under conditions of the non-adiabatic creation of RP, the populations of the spin states of separated pairs will be different: $\rho_{\alpha\alpha,\,\alpha\alpha} = \rho_{\beta\beta,\,\beta\beta} = 1/3$ $\rho_{\alpha\beta,\,\alpha\beta} = \rho_{\beta\alpha,\,\beta\alpha} = 1/6$. ST_0RPM CIDEP results in overpopulating of the $|\alpha\beta;\,\chi\rangle$ spin state in comparison to the $|\beta\alpha;\,\chi\rangle$ spin state for parameters used in **Figure 6**: $\rho_{\alpha\beta,\,\alpha\beta} = 1/6 + \delta$ and $\rho_{\beta\alpha,\,\beta\alpha} = 1/6 - \delta$ where $\boldsymbol{\delta} > 0$. The most remarkable thing that follows from **Figure 6** is an admixture of adiabaticity to the nonadiabatic populating of the RP spin states which lead to the same result.

3.2. History. The Closs-Forbes-Norris (CFN) model

In 1987, Closs et al. [73] suggested a model (CFN) for an SCRP diffusing within heterogeneous inhomogeneities, with sizes on the nanometer scale, for example, for micellized SCRPs or for organic biradicals with paramagnetic centers connected via a flexible tether. A highly significant distinction of the CFN model from the QSA one is that the electron spin-spin exchange interaction is considered to be a time- and space-independent "effective value," called J_{eff}. The diagram in **Figure 6** illustrating the origin of APS in terms of QSA is replaced by the spectral characteristics (**Table 1** where *J* is considered as time and distance independent J_{eff}) of the effective spin Hamiltonian to explain the origin of APS in terms of CFN. In fact, the CFN model operates with the averaged Hamiltonian, that is, in the limit of fast motion. This assumption greatly simplifies the interpretation of TREPR spectroscopic data collected for a confined SCRP. In calculating spectra using the CFN model, there is no need to average the spectra over the distribution of diffusional distances between radicals at the moment of observation. The model eliminates the

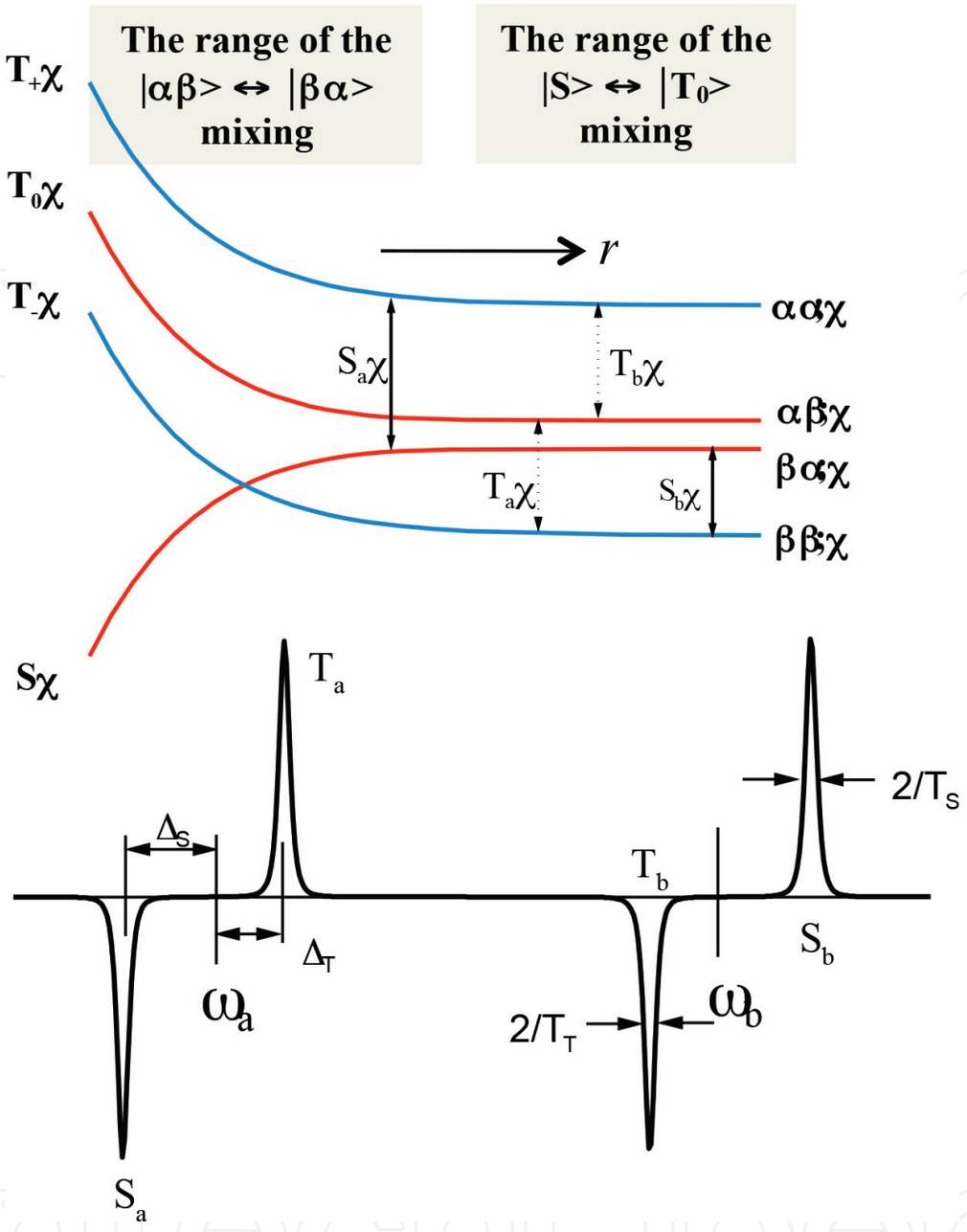

Figure 6. A correlation diagram for the spin energies of an SCRP as a function of the distance r between the radicals at a given configuration χ of the nuclear spins. The exchange potential is assumed to depend on the distance r in an exponential manner. The spectra below the correlation diagram illustrate the classification and the labeling of the TREPR transitions in a radical pair (from low to high fields, these are S_a, T_a, T_b, and S_b).

most problematic aspects of the QSA approximation. But there is a new problem—what is the effective exchange interaction J_{eff}? How is it defined? Moreover, the problems of the simultaneous occurrence of CIDEP due to the RPM, as well as the problem of line widths of the APS components, remained unsolved.

The undoubted success of the CFN model is that it is able to explain the dominance of APS in the CIDEP patterns in the TREPR spectra of confined SCRPs. Due to its physical clarity, the CFN model has enjoyed impressively wide applications [75–80].

http://dx.doi.org/10.5772/67463

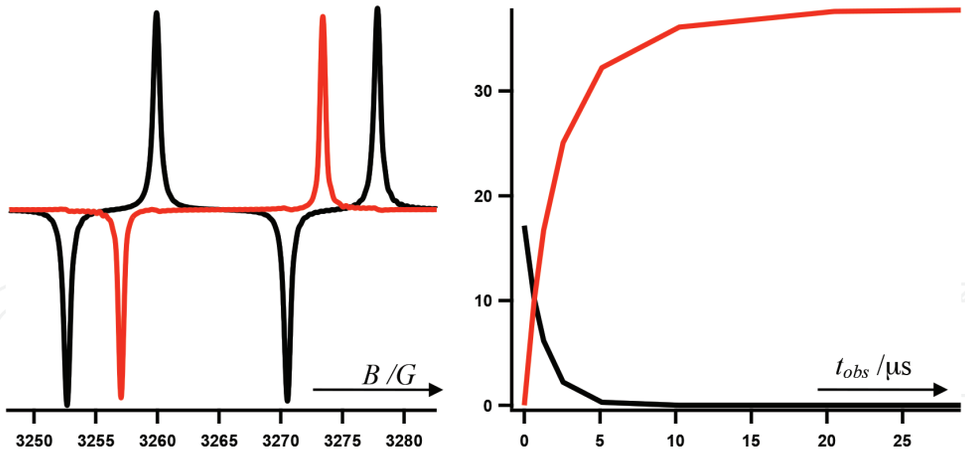

Figure 7. Decay ($k_t = 6.4\times10^5$ s^{-1}) of the CFN pair (solid line) and generation of the RPM–like CIDEP (dashed line). Spectral shapes of observed TREPR signals (left) at $t_{obs} = 0.8$ μs (solid) and $t_{obs} = 256$ μs (dashed); and their kinetics (right): APS- (solid) and RPM-like (dashed) CIDEP in escaped radicals. |Jeff/q| = 0.05. The initial spin state of RP is assumed to be a triplet with equal populations of the $|T_+>$, $|T_->$ and $|T_o>$ spin states.

However, as new experimental observations become available, it was gradually recognized that the CFN model fit experimental data only under certain conditions. For example, rather surprisingly, J_{eff} was found to depend on temperature [81, 82] and on the chemical structure [83] of the detergent making up the micelle. The model failed to explain the dependence of the width of the spectral lines on micelle's size [82, 84, 85] or on the length of the hydrocarbon tether [86] connecting two paramagnetic centers in biradicals. Moreover, it was not clear if the importance of the compartment size arises from the space dependence of the exchange and dipolar interactions or on other factors. It must be underscored that the line widths of radical pairs were found [82, 84, 85] to be noticeably larger than those of the "escaped" ones, despite both radicals, paired and escaped, being located in the same micellar phase. This difference in line widths was found to be dependent on micellar size as well.

3.3. The CFN model: decay of the pair spin system

The assumption that the CFN spin system can decay or transform due to chemical or physical processes makes the application of the model wider and the model itself more realistic.

The initial CFN system, comprised of spins ***a*** and ***b*** and characterized by inter-radical interaction $\hat{V}_{ab}$, can be converted by a chemical reaction into a secondary CFN with a rate constant k_t. The secondary CFN is comprised of the spins ***A*** and ***B*** with the inter-radical interaction $\hat{v}_{AB}$. Such a process is described by the Liouville equation (10):

$$\begin{pmatrix} \dot{\boldsymbol{\rho}}_{ab} \\ \dot{\boldsymbol{\rho}}_{AB} \end{pmatrix} = \begin{pmatrix} -i\hat{\hat{H}}_{ab} + \hat{\hat{H}}_{\mu;ab} + \hat{\hat{R}}_{ab} - k_t \cdot \hat{\hat{E}} & \hat{\hat{0}} \\ k_t \cdot \hat{\hat{E}} & -i\hat{\hat{H}}_{AB} + \hat{\hat{H}}_{\mu;AB} + \hat{\hat{R}}_{AB} \end{pmatrix} \cdot \begin{pmatrix} \boldsymbol{\rho}_{ab} \\ \boldsymbol{\rho}_{AB} \end{pmatrix} \qquad (10)$$

If radicals ***A*** and ***B*** do not interact ($\hat{v}_{AB} = 0$), then they become free radicals or "escaped." From Eq. (10), the corresponding TREPR spectra are shown in **Figure 7**. The TREPR spectrum of the new CFN pair (**Figure 7**, left-hand, dashed line), comprised of non-interacting radicals, is

identical to that what is called CIDEP due to the ST_0RPM. In fact, in this calculation, we have reproduced the so-called exponential model of CIDEP. This model is considered to be absolutely unrealistic for the generation of CIDEP in a chemical reaction resulting in geminate radical pairs, but here, we deal with a CFN pair as a precursor and its conversion to the secondary one. For the CFN pair, the effective exchange interaction is allowed to be arbitrary small, which makes it probable that the decay of the CFN polarization is followed by the creation of CIDEP, similar to what is induced by the exponential model like CKO as applied to CIDEP.

4. Diffusion models for APS

4.1. SCRPM versus ST_0RPM

In order to address some of the deficiencies inherent to the QSA, in 1991, Shushin [38] suggested a diffusive theory for SCRP-induced CIDEP in homogeneous solvents. Instead of the QSA, Shushin considered a solution to the Stochastic Liouville Equation (SLE) as applied to freely diffusing radicals. The evolution of the SCRP total spin ($\hat{\mathbf{S}} = \hat{\mathbf{S}}_a + \hat{\mathbf{S}}_b$) is governed by the spin Hamiltonian Eqs. (4)–(6). The main difference between the QSA and SLE approaches is that the averaging of the spectra corresponding to the instantaneous spin Hamiltonians in the QSA is replaced by an averaging of the pair-spin density matrix over stochastic diffusional processes governed by the SLE.

The model is correct for $t_{obs} \gg T_2$ or for $\bar{r} \gg \sqrt{DT_2}$, where $\bar{r}$ is average distance between radicals at $t = t_{obs}$ and $D = D_a + D_b$ is the coefficient of their mutual diffusion. Shushin's model is much more than a refined treatment of the problem. In fact, it drastically changed the qualitative interpretation of the APS by experimentalists. Now, not only do the interacting radicals contribute to the APS but also there are additional contributions from radicals which interacted in the past and yet do not interact at the moment of observation. This is seen from the analytical expression [38] for the line shape of the TREPR signal at t_{obs}:

$$I(\omega) \cong 2\pi \cdot P_{ST}\left(\frac{T_2}{1+T_2^2(\omega-\omega_a)^2}-\frac{T_2}{1+T_2^2(\omega-\omega_b)^2}\right) - 4\pi^2 P_0 D\lambda \cdot \left[\frac{T_2^3(\omega-\omega_a)}{\left(1+T_2^2(\omega-\omega_a)^2\right)^2}+\frac{T_2^3(\omega-\omega_b)}{\left(1+T_2^2(\omega-\omega_b)^2\right)^2}\right] sign(J) \tag{11}$$

where P_{ST} is the enhancement factor of CIDEP due to ST_0RPM and P_0 can be interpreted as a concentration of contact SCRPs. The term $1/T_2$ is the Lorentzian line width, including exchange broadening. From Eq. (11), the TREPR spectrum of a SCRP is comprised of two distinguishable parts: (1) multiplet ST_0RPM polarized Lorentzian EPR signals centered at the resonance magnetic fields of the individual free radicals ($\boldsymbol{\omega}_a$ and $\boldsymbol{\omega}_b$) and (2) two APS-split signals which are simply the first derivatives of the Lorentzian lines centered at the individual free radical resonances. The amplitude of these APS-split signals is proportional to the concentration of SCRPs present at t_{obs} that still have an opportunity for a re-encounter. The radicals that have lost this opportunity contribute to the ST_0RPM polarization.

http://dx.doi.org/10.5772/67463

What immediately follows from Shushin's diffusion model is the dominance of the polarization due to ST_0RPM, even at the shortest possible times of observations (~100 ns). Using representative parameters, the relative intensity of the APS is no more than 0.1%. Such a small distortion of the ST_0RPM polarized signal cannot be discerned in an ordinary *cw* TREPR experiment. It can therefore be stated with confidence that except for the central line of a spectrum, where the ST_0RPM contribution approaches zero, it is impossible to detect an APS in ordinary liquid solutions.

At first glance, this conclusion contradicts many experimental observations [87]. However, Tominaga et al. [87] came to the conclusion that at low temperatures (< −70°C), there exist solvent/solute structures in *i*-propanol/acetone mixtures which persist for a few microseconds and that the guest ketyl radicals are fixed in these structures by means of hydrogen bonding to the host *i*-propanol molecules. This is in reasonable agreement with the suggestion [88] that geminate radical pairs can be trapped in a spherically symmetric potential hole and diffuse freely within it.

4.2. The Microreactor model for the micellized radical pair

By itself, the microreactor model [89, 90] was formulated to explain [91] the extremely high efficiency [92] of the magnetic isotope separation in chemical reactions of geminate radical pairs confined in a micellar phase. Essentially, the model is a synthesis of mathematical formalism [31–33] developed to account for the spin dynamics of radical pairs, with a particular model for diffusion-controlled reactions in micellar media [93, 94]. To make the model workable, we make two assumptions: (1) the microreactor model approximates the micelle as a spherical homogeneous drop of radius L_m (**Scheme 4**) and (**2**) One radical from the pair, of radius r_a, is considered to be fixed at the center of the micelle, while the other, of radius r_b, is allowed to diffuse and to escape from the micelle to the water bulk.

The theory of the TREPR spectroscopy of SCRP is described in details in references [84, 85].

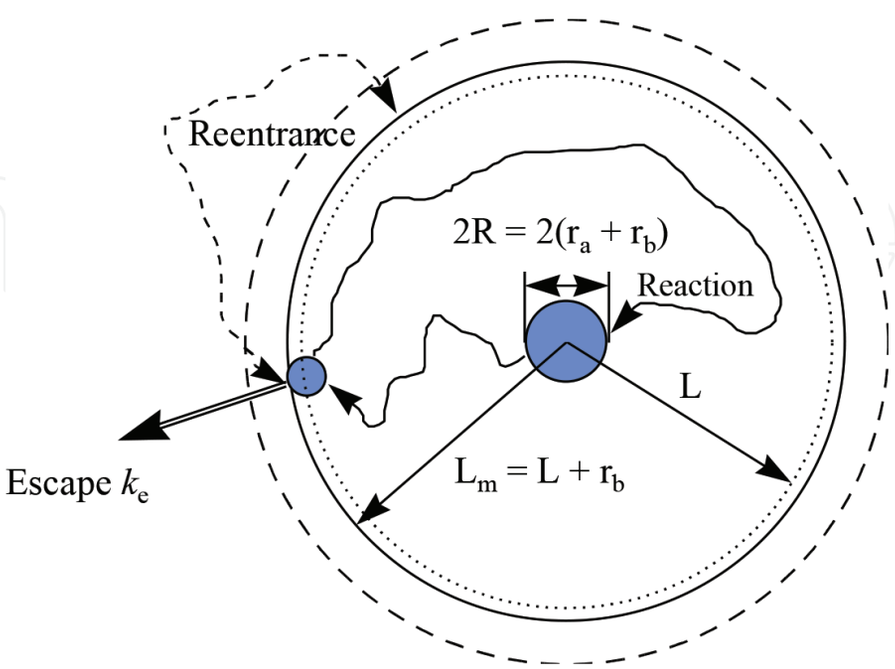

Scheme 4. Visualization of the microreactor model for SCRPs.

5. Micelle size dependence

5.1. Photolysis of methyl desoxybenzoin (MDB) [84]

Here, we present an example that demonstrates the high sensitivity observed for the APS in the ^{13}C-benzoyl radical as a function of the size of its alkyl sulfate micellar host. Moreover, it has been found that a decrease in micelle size results in a strong asymmetry of the observed APS.

Upon photoexcitation (**Scheme 5**), the ketone MDB dissociates into a triplet SCRP consisting of benzoyl and sec-phenethyl radicals (**Scheme 5**).

The TREPR spectra obtained for this system at $t_{obs} = 500$ ns after the laser flash ($\lambda = 308$ nm) are shown in **Figure 8**. The dominant feature here is the $m_N = \pm$½ doublet from the ^{13}C-benzoyl radical, with a hyperfine coupling constant on the ^{13}C carbonyl, A(^{13}C) = 127 G. Each line in this doublet is a superposition of the APS from the SCRP and ST_0RPM polarized signal from free (escaped) radicals. In the latter, the $m_N = +1/2$ line is in emission; the corresponding $m_N = -$½ line is in absorption (the E/A pattern). The SCRPM contribution dominates at the early delay times and in large micelles. The ST_0RPM is more prominent at the longer delay times and in small micelles. Note that as predicted above, the broad APS-split signals show no ST_0 polarization.

The Δ_{APS} splitting (defined as the distance between the extremes of the APS) was found to increase when the micelle size decreases: 0.85 mT in SDS (C_{12}), 1.42 mT in undecyl sulfate (C_{11}), and 1.58 mT in decyl sulfate (C_{10}) micelles. Also, the two lines comprising the APS have different intensities. Except for the C_{12} micelles, where the APS is almost symmetric, the T-type lines are stronger and narrower than the S-type partners. This asymmetry is more prominent in smaller micelles. The shape of the APS pattern was found to be independent of the delay time t_{obs} and the amplitude of microwave field ($\omega_1 = (0.01 - 2) \times 10^6$ rad/s). The E/A-polarized lines of the benzoyl radicals are much narrower than the width of the APS components (0.06 mT vs. 0.8–1.5 mT).

The parameters used in our calculations using the microreactor model are given in **Table 2**, where σ is the boundary factor describing the probability for radicals to escape from the micelle core and P is the reaction probability of the SCRP ($P = P_r + P_d$; to elaborate, the terms P_r and P_d are the probabilities for recombination and disproportionation of the radicals, respectively). We can measure these values directly using racemization of the optically active MDB and by measuring the chemical yield of benzaldehyde. The term $Z = \frac{3RD}{L^3 - R^3}$ [84] is the

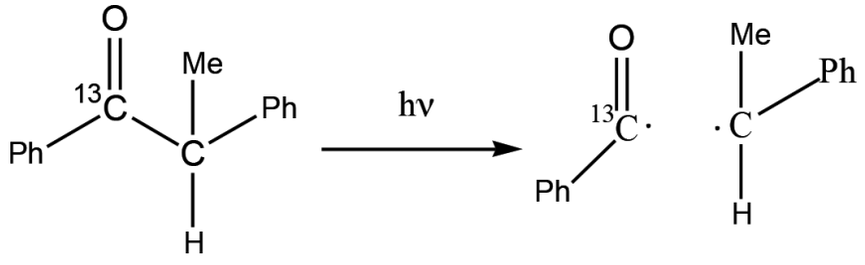

Scheme 5. Photolysis of MDB results in formation of the triplet SCRP consisting of benzoyl and sec-phenethyl radicals.

http://dx.doi.org/10.5772/67463

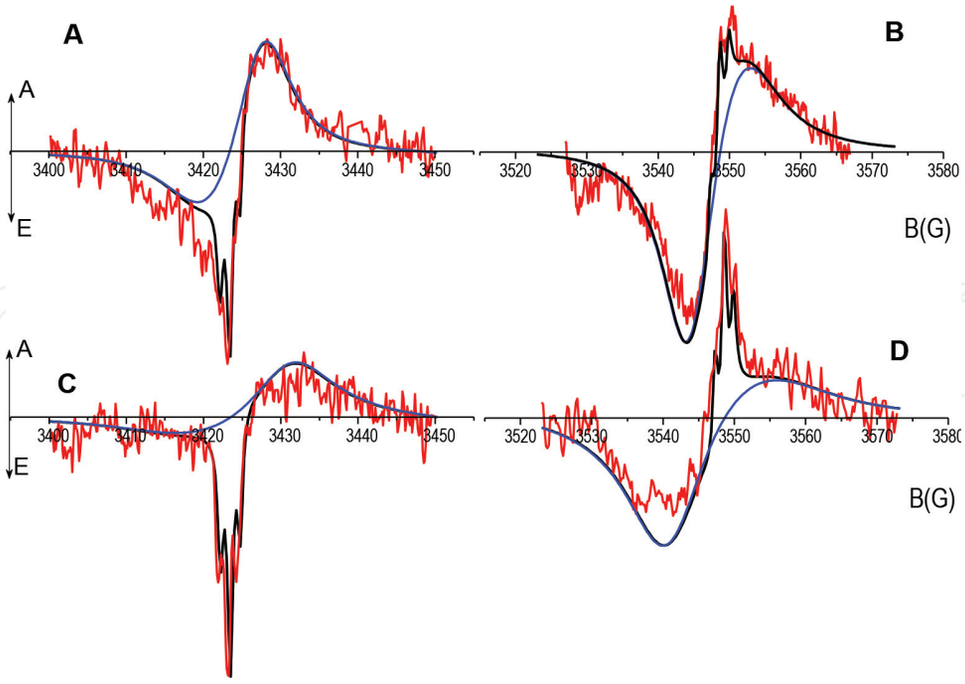

Figure 8. TREPR spectra observed in laser photolysis of MDB in sodium dodecyl (A and B) and in sodium decyl (C and D) sulfate micelles (open circles). Only $M_N = +½$ (A and C) and $M_N = –½$ (B and D) signals from ^{13}C–benzoyl radicals are shown (hfi constant A(^{13}C) = 127 G). The transverse magnetization $M(t)$ was convoluted with $f_1(t) = (t/\tau_w^2)exp(–t/\tau_w)$; $\tau_w = 500$ ns according to window fuction used in simulations. Simulated spectra (bold lines) were calculated using the model of microractor. Dashed lines represent TREPR spectra of radical pairs inside the micelles.

n[a]	Δ_{APS} (mT)	$L \times 10^8$ cm[b]	$D \times 10^6$ cm^2/s	σ	P[c]	$Z \times 10^{-7}$ s^{-1}	$J_o\tau_{EX}$ [d]	$J_0\lambda^2/D$	$A/4Z$
12	0.85	15.4	1.58	0.022	0.51	8.28	2.43	0.20	26.6
11	1.42	14.2	2.02	0.018	0.53	13.7	1.90	0.16	16.1
10	1.58	12.9	2.50	0.015	0.51	23.3	1.54	0.13	9.44

[a]The number of carbon atoms in the detergent chain.
[b]The choice of the value of L is discussed in [94]; note, that the actual micellar size $L_m = L + r_b$ (see **Scheme 4**).
[c] This is total reaction probability including the recombination and disproportionation.
[d]$J_0 = -2.2 \times 10^{10}$ rad/s, $\lambda = 0.5 \times 10^{-8}$ cm, $R = 6 \times 10^{-8}$ cm.

Table 2. Parameters used in simulations in **Figure 8** and representative values.

frequency of forced encounters of radicals in the micellar phase; $J_0\tau_{ex}$ [84] and $J_0\lambda^2/D = J_0\tau_c$ [84] are parameters characterizing the efficiency of spin exchange.

5.2. Photolysis of dimethyl desoxybenzoin (DMDB) [81]

The photolysis of DMDB is illustrated in **Scheme 2**. The TREPR spectra acquired at $t_{obs} = 300$ ns are shown in **Figure 9**. Qualitatively, the observed spectra from MDB and DMDB are similar (compare **Figures 8** and **9**). However, the quantitative conclusions are different. Micelle sizes extracted from simulations of SCRP and TREPR spectra, resulting from the photolysis of MDB and DMDB are practically same as that for SDS micelles—$L = 15.4$ Å for MDB and 15.7 Å for

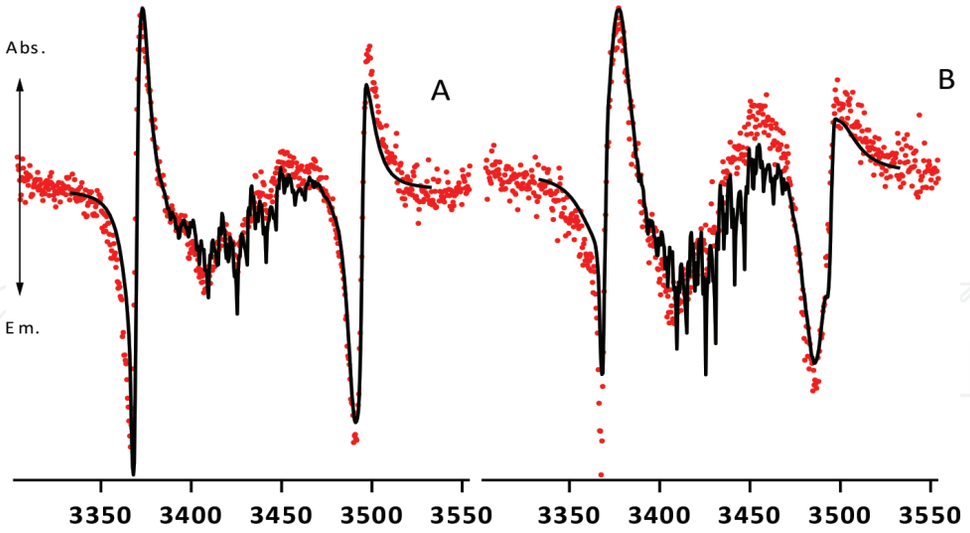

Figure 9. Time–resolved ESR spectra observed (open circles) in 308 nm laser photolysis of DMDB (2 mM): (A) in SDS (0.1 M); (B) in decyl sulfate (SDeS) (0.21M) micelles. The calculated spectra are represented by solid lines. Parameters used for the simulations are; $J_0 = -2.4\times10^{10}$ rad/s, $\lambda = 0.5$ Å, $R = 6$ Å, L(SDS) = 15.7 Å, L(SDeS) = 11.6 Å, D(SDS) = 0.7×10^{-6} cm^2/s, D(SDeS) = 1.2×10^{-6} cm^2/s. (a – ^{13}C–benzoyl) A_a[CO] = 127 G, $g_a = 2.0006$, $g_b = 2.0026$; $T_{1a} = 0.1$ μs, $T_{1b} = 3.0$ μs, $T_{2a} = 0.08$ μs, $T_{2b} = 1.6$ μs, $\tau_w = 0.3$ μs.

DMDB. However, in the case of SDeS, they differ significantly: $L = 12.9$ Å for MDB and 11.6 Å for DMDB. Diffusion coefficients were found to be different as well: $D = 1.08 \times 10^{-6}$ cm^2/s and 2.5×10^{-6} cm^2/s in SDS and SDeS in the case of MDB and respectively, 0.7×10^{-6} cm^2/s and 1.2×10^{-6} cm^2/s for the case of DMDB.

Comparing these values, one has to keep in mind that the sec-phenethyl radical is more hydrophilic and less bulky than the cumyl radical. This easily explains the differences obtained for the diffusion coefficients. As far as the micelle size difference is concerned, the difference in hydrophobicity is the main reason. Indeed, the higher the hydrophobicity of the radical, the smaller the range available for radical diffusion inside the micelle. Of course, the smaller the micelle size, the stronger the influence of this factor.

At the present stage of both experimental and computational analysis, it is rather difficult to make conclusions as to how we could estimate the importance of these differences between MDB and DMDB. Further investigations are necessary. Nevertheless, the observed differences give a fairly good reason to consider the TREPR spectroscopy of spin-correlated radical pairs to be a very sensitive method for studying diffusional mobility and the characteristic sizes of the inhomogeneities where the spin-correlated pairs are localized.

5.3. Photolysis of (2,4,6-trimethylbenzoyl)-diphenylphosphine oxide (TMDPO) [85]

The photoexcitation (**Scheme 6**) of TMDPO leads to the formation of a geminate triplet SCRP of diphenyl phosphonyl and 2,4,6-trimethylbenzoyl radicals via dissociation of a short-lived triplet state (lifetime less than 1 ns) of TMDPO.

There are three distinctive features of the spectra in **Figure 10**: (1) the diphenyl phosphonyl radical possesses one of the largest known hyperfine coupling constants (385 G) in the family of "organic" radicals. This allows for the manifestation of the so-called ST_RPM CIDEP [85],

http://dx.doi.org/10.5772/67463

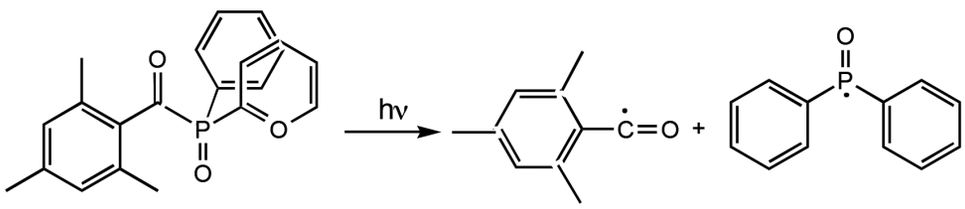

Scheme 6. Photolysis of TMPBPO.

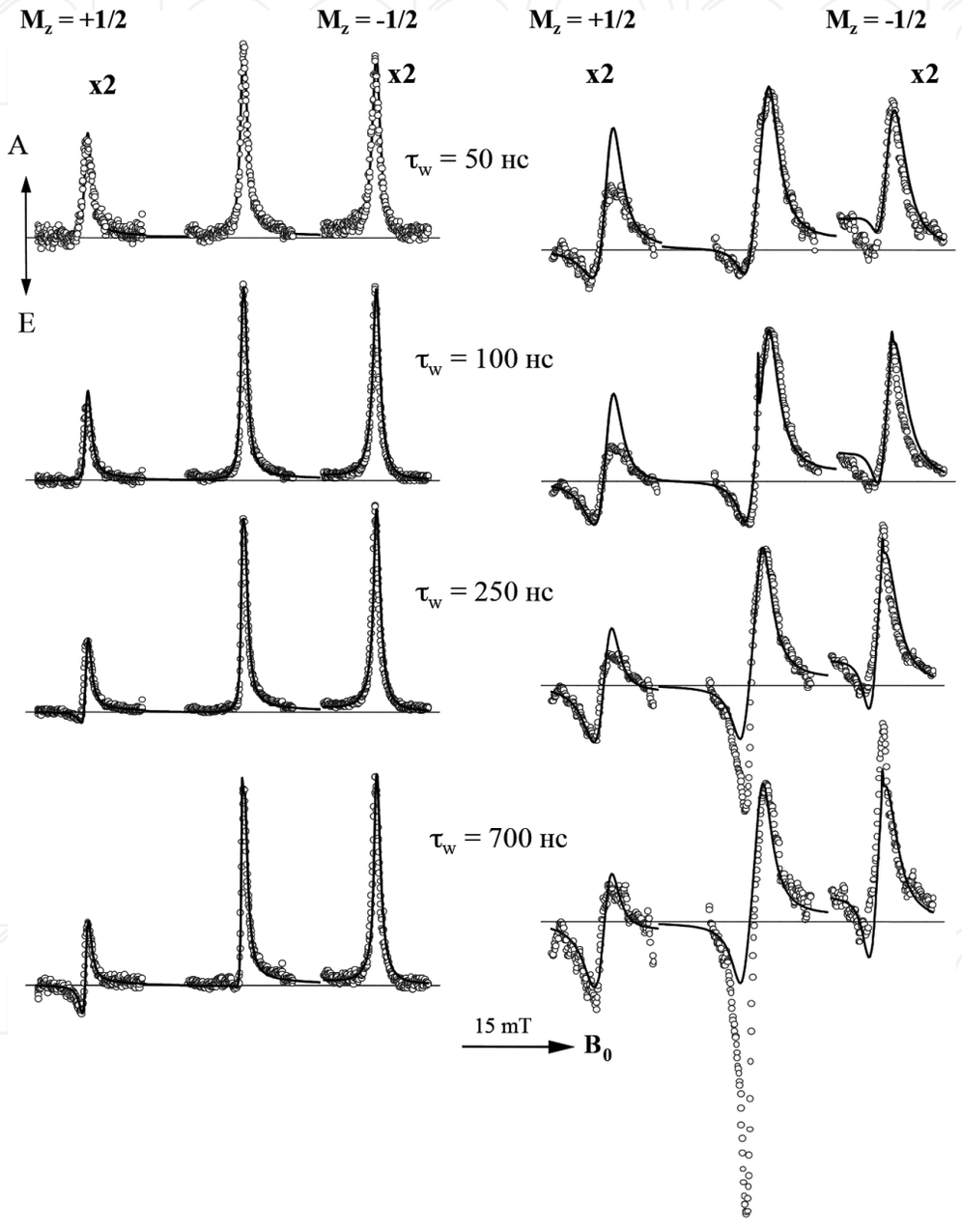

Figure 10. The TREPR spectra observed during 308 nm laser photolysis of TMDPO in SDS (C_{12}) and in sodium octylsulfate (C_8) micelles. The parameter t_w is the gate width of the t-exponential window. The intensities of the $m_P = \pm 1/2$ lines from the diphenyl phosphonyl radical have been enlarged by a factor of two for convenience. The simulated spectra are calculated using the microreactor model and are shown by solid lines. Flip-flop electron-nuclear spin transitions were taken into account to simulate ST_RPM polarization with a distance-dependent exchange potential. Parameters used in this simulation are given in **Table 3**. The term Δ_{APS} is defined as the splitting, measured in Gauss, between the extremes of the APS.

even in the relatively high-field X-band experiment (0.34 T). (2) This is the first observation of a competition between the SCRPM and the ST_RPM. We have already mentioned that the ST_0RPM CIDEP is not seen when the SCRPM dominates; SCRPs from MDB and from DMDB photolysis do not show a ST_0RPM contribution (**Figures 8** and **9**). But at the same time, escaped radicals demonstrate ST_0RPM CIDEP and do not show any SCRPM (APS). It is rather intriguing that there is competition between the SCRPM and the ST_RPM and yet simultaneously no competition between the ST_0RPM and the SCRPM. (3) At initial observation times, the pair is strongly TM polarized. The evolution of the TM CIDEP to the ST_RPM through the SCRPM is extremely sensitive to the micelle size, as **Figure 10** convincingly demonstrates.

It is also interesting to note that changing parameters such as diffusion coefficients and microreactor sizes follows the same logic established by comparing these parameters to the cases of MDB and DMDB (see **Figure 9**, **Table 2**, and surrounding discussion).

5.4. Photooxydation of glycyl-glycine (GG) by the electronically excited triplet state of anthraquinone-2,6-disulfonate (AQDS) in AOT reverse micelles [95]

Figure 11 shows the TREPR spectra obtained during the photoexcitation of anthraquinone-2,6-disulfonate (AQDS) in the presence of diglycine (GG) where both the photosensitizer and the substrate are confined to the aqueous interior of AOT reverse micelles (**Scheme 7**). A remarkable feature of these spectra is the observation of the superposition of two CIDEP patterns, APS and ST_0RPM. The ST_0RPM polarization observed here does not have the appearance of spectral lines expected of free radicals as an addition to APS (cf. **Figure 8**). In this particular case, the contribution of ST_0RPM is seen as an increase in the intensities of the S-type components of APS, that is, the ST_0RPM polarization belongs to the SCRP indeed but not to the free radicals that have escaped from the water core into the bulk solvent (n-octane), with subsequent localization in other reverse micelles.

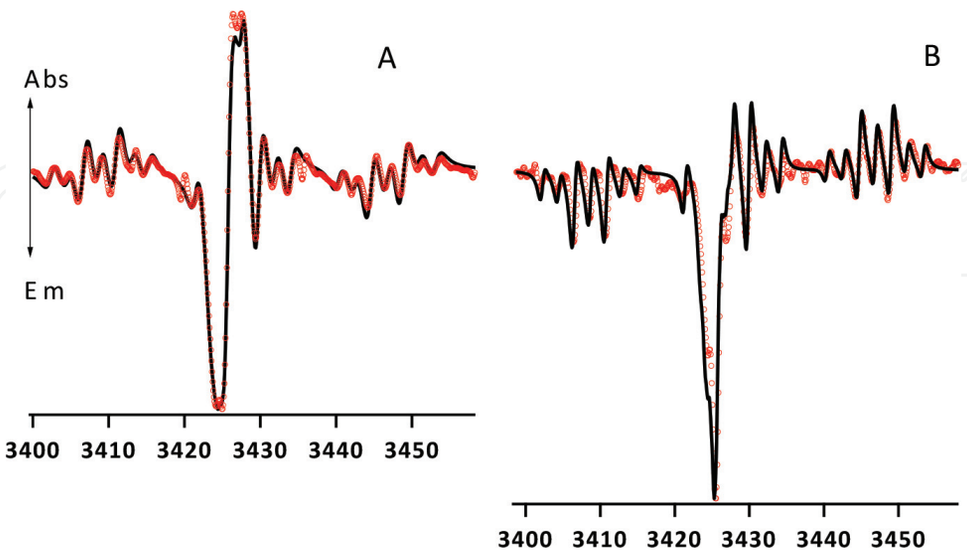

Figure 11. TREPR spectra (empty circles) observed under photooxidation (laser flash photolysis, $\lambda = 308$ nm) of GG by AQDS in AOT micelles for L_m values of 23 Å (A) and 53 Å (B), at room temperature. Solid lines are simulations in terms of the microreactor model.

http://dx.doi.org/10.5772/67463

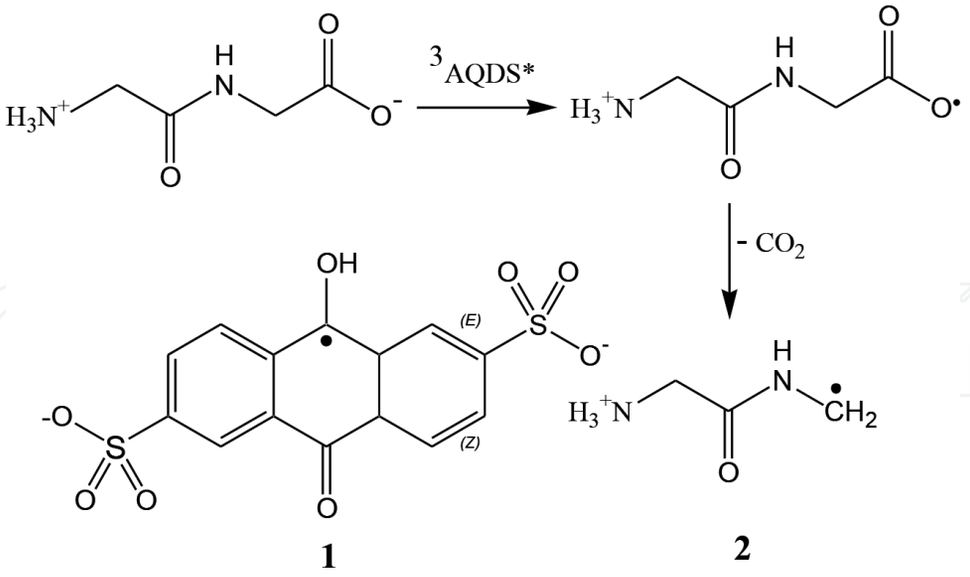

Scheme 7. Generation of geminate triplet radical pair 1…2 under the photolysis of AQDS in AOT reverse micelles.

Simulations of the TREPR spectra of SCRPs in alkyl sulfate micelles showed that the viscosity of the micellar phase decreases with the micelle size. AOT micelles seem to behave differently. A decrease in the water core radius from 53 Å to 17 Å causes a decrease in the mutual diffusion coefficient from 2.4×10^6 cm^2/s to 0.05×10^6 cm^2/s. This is in reasonable agreement with other measurements reported from fluorescence depolarization experiments [98], that is, the aqueous interior of reverse micelles becomes more viscous as its size decreases. It is speculated that the decrease in size is accompanied by a greater degree of ordering of the solvent.

Another remarkable observation is that the ST_0RPM contribution dominates in the micelles with an extremely low frequency of forced encounters $Z = 5.2 \times 10^6$ s^{-1}, compare with the lowest frequencies $Z = 8.28 \times 10^7$ s^{-1} in the case of MDB in SDS and $Z = 2 \times 10^7$ s^{-1} in the case of TMDPO in SDS. Whether this finding makes physical sense is less important, at least at present, than recognizing that the peculiar distortion of the APS by the ST_0RPM can be a very sensitive measurement tool for the sizes of inhomogeneities on the nanometer scale.

6. Temperature dependence: photoreduction of benzophenone in SDS micelles [82, 96]

From the point of view of the CFN model and QSA, the temperature dependence of the APS is quite unexpected. Indeed, the QSA operates in terms of the distance dependent on exchange potential and always in regard to a particular distribution of radicals at the time of observation. Neither of these can change the shape of APS but both can drastically alter its intensity. The CFN model utilizes the concept of an effective exchange interaction, but the model's temperature dependence is not immediately clear.

The radical structures under consideration are shown at the top of **Scheme 8**. The photoreduction of the excited triplet state of BP (^{3}BP*) in SDS [97] results in a triplet-born SCRP consisting of

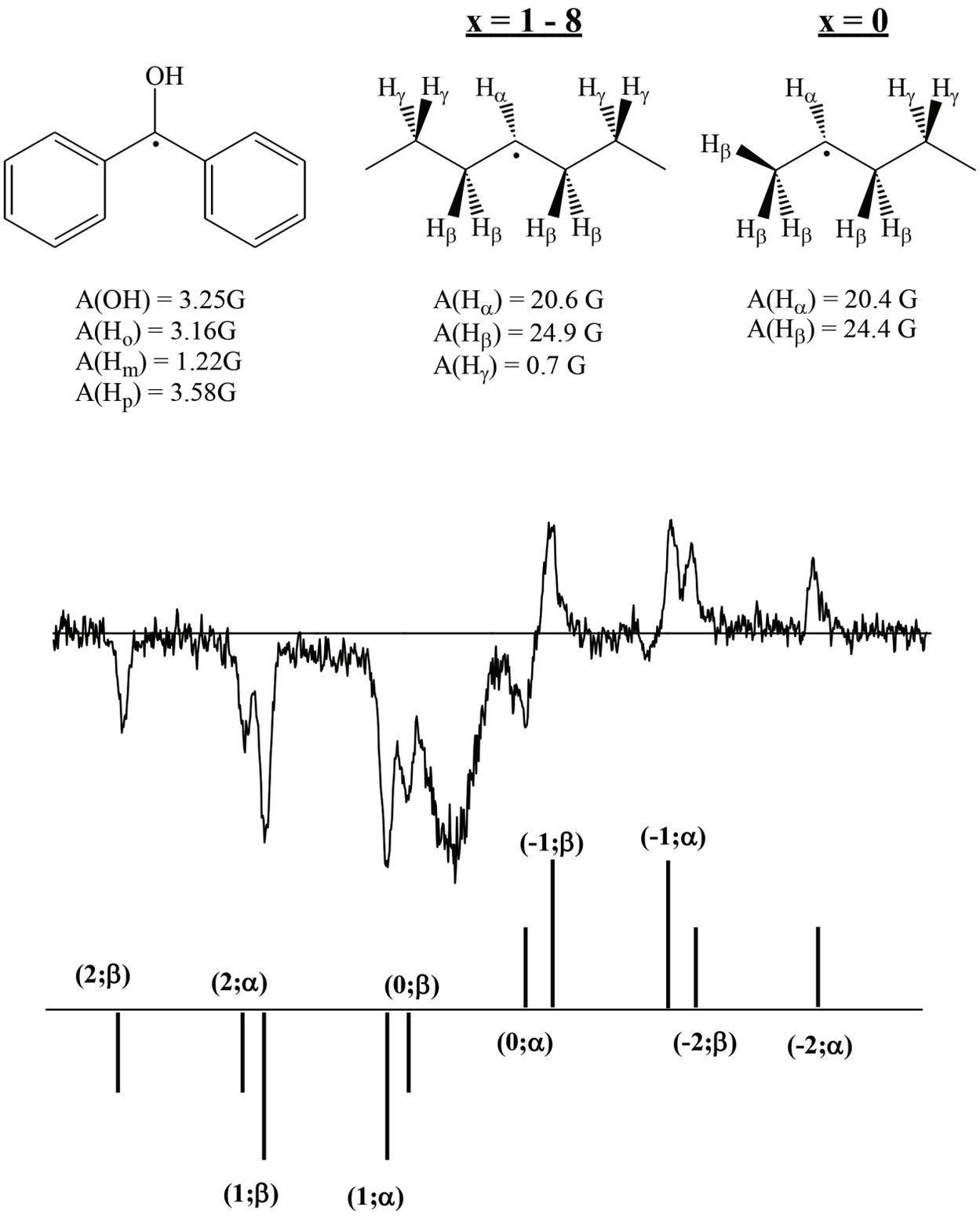

Scheme 8. Stick plot (bottom) of the TREPR transitions expected for the primary alkyl radical products from the photochemical reduction of the alkyl chain of a surfactant by a triplet sensitizer (top). A TREPR spectrum of the escape radicals of SDS is shown in the middle.

http://dx.doi.org/10.5772/67463

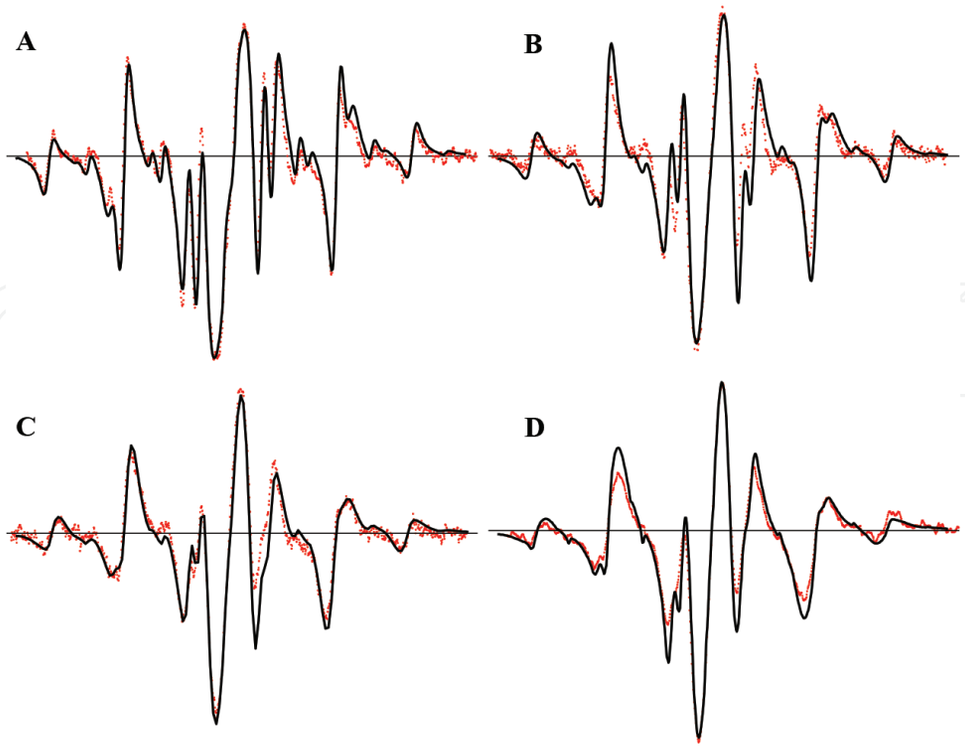

Figure 12. TREPR spectra observed during 308 nm laser photolysis of BP/SDS (open circles), acquired at a 500 ns delay time (gate width of the boxcar window was 100 ns), at 16°C (A), 32°C (B), 46°C (C), and 60°C (D). Simulated spectra (the t–exponential sampling window is centered at 500 ns) were calculated using the microreactor model and are designated by solid black lines. Parameters used in the simulations are listed in **Table 5**.

surfactant-based secondary alkyl radicals of the general structure $CH_3(CH_2)_n\dot{C}H(CH_2)_{10-n}OSO_3^-$ ($n = 0$–9) and the BP ketyl radical ($Ph_2\dot{C}OH$). **Figure 12** shows simulations of the experimental spectra for this system in terms of a numerical solution of the SLE as applied to the microreactor model. Despite some rather simple but necessary simplifications, the model is capable of reproducing all of the key features of the experimental spectra and all of the observed temperature effects. Specifically, these are [82, 91]: (1) increasing the temperature causes broadening of the APS components, (2) the strong line shape asymmetry in the APS spectral pattern depends on the q values, (3) narrowing of the central portion of the spectra takes place with increased temperature, and (4) narrowing of the line widths of the escaped alkyl radicals is observed. The parameters used in the calculations are presented in **Table 3**. All the values are in reasonable agreement with available data from other experiments. In general, the temperature effect was very similar to that of reducing the size of micelles. This suggests that molecular translational mobility, and its restrictions, is the key factor in determining the spectral shape of the APS in the TREPR spectra of SCRPs experiencing limited mobility. The dependence of the asymmetry phenomenon on the value of q is a fundamental issue to be addressed for future applications of SCRPs as spin-polarized probes.

We have successfully demonstrated that the TREPR spectra of SCRPs, coupled with simulations in terms of the microreactor model, can be used to investigate the sizes and internal viscosities of

Temp. ±0.5°C	L[b] (Å)	$D\times10^{-7}$ (cm^2/s)	$A[H_\beta]$[c] (G)	T_{2a}[d] (μs)	$k_{rel}\times10^8$ (s^{-1})[e]	$k_g\times10^6$ (s^{-1})[e]	$Z\times10^7$ (s^{-1})	$J_0\lambda R/D$ ($J_0\lambda^2/D$)	$q(0,\alpha)/Z$
16	17.2	2.0	24.9	0.080	2.0	2.2	0.74	36 (3)	3.1
32	16.3	3.5	24.6	0.095	3.3	4.5	1.5	21 (1.8)	1.5
46	15.6	5.3	24.4	0.107	4.8	7.8	2.7	14 (1.2)	0.84
60	14.6	8.0	24.2	0.120	6.8	13	4.8	9.0 (0.8)	0.47

[a]Temperature independent parameters: $J_0 = -2.4 \times 10^{10}$ rad/s; $\lambda = 0.5$ Å; $R = 6$ Å; $D_{ZFS} = 3.4 \times 10^{10}$ rad/s [41]; $\sigma = 0.024$; $\Lambda_s = 0.62$; $\eta = 0.2$; $g_a = 2.0026$; $g_b = 2.0028$; $\omega/2\pi = 9.8$ GHz; and $\omega_1 = 10^5$ rad/s.
[b]The variation of L within 0.4 Å at 16°C and 0.2 Å at 60°C is fairly acceptable. In **Table 1**, the upper limit values are presented. All other parameters are those that have been used with the presented L values. Note that L is the radius of spherical volume available for radicals. Thus, the real micelle size is greater by approximately 3 Å.
[c]The hyperfine coupling constant with the H_α protons in the $n = 1$–8 fragments do not seem to vary noticeably with temperature.
[d]T_{2b} was assumed to be the same (see text). T_{1a} and T_{1b} were also assumed to be the same and independent of temperature. It is likely that this is incorrect, but the spectral shape is insensitive to these parameters when they are varied within reasonable limits.
[e]k_g and k_{rel} are the rates respectively of the hydrogen abstraction and relaxation of the polarized triplet state of benzophenone.

Table 3. Parameters[a] used to simulate the TREPR spectra of alkyl/ketyl RPs in SDS micelles at different temperatures.

inhomogeneous structures on the nanometer scale. Such experiments convincingly show that they can be a source of valuable information on the inter-radical interactions as well. However, even successful simulations bring an aesthetic satisfaction without increasing our knowledge of the physical characteristics of the system. In the next section, we will try to resolve this deficiency.

7. Random walks in micelles: ST_0RPM versus SCRPM

Our experimental observations and their successful simulations in terms of the microreactor model teach us that in alkylsulfate micelles, the ST_0RPM polarization is observed only for escaped radicals, while in AOT reverse micelles, the ST_0RPM can be either negligible or dominating. In homogeneous solution, the ST_0RPM undoubtedly dominates the TREPR spectra. This is easily demonstrated using the microreactor model for large values of L_m. This point is crucial, as the early theories of CIDEP addressed precisely the case of radicals that never experienced repeated collisions after they were involved in the creation of polarization. Mathematically, this is realized through the calculations of reduced spin density matrices by the *Tr* operation. Calculations in terms of the microreactor model show that the observed ST_0RPM polarization is present not only in the radicals released from the medium but also on those inside of it, if the values of L_m and the viscosity of micelle core are sufficiently large (compare, for instance, the values of these parameters given in **Tables 4** and **5**).

Analytical solutions to the problem of mutual diffusion of two particles, within a closed volume on the nanometer scale, exist only for the particular case of a spherically symmetric compartment, with one of the partners fixed in the center of the sphere [89, 90, 93]. Instead, we apply the Random Walks (RW) model to integrate the SLE as applied to an SCRP confined in a

n	Δ_{APS}[a] (mT)	k_{obs}[a] $\times 10^7$ (s^{-1})	L[b] (nm)	D[b] $\times 10^6$ (cm^2/s)	η[b]	T_{1a}[b] (ns)	Z[c] $\times 10^{-7}$ (s^{-1})	$-J_0\tau_{ex}$[c]
12	0.85±0.04	1.0±0.2	16.0	0.44	0.44	90	2.70	30.0
11	1.19±0.04		15.2	0.51	0.41	80	3.70	25.9
10	1.60±0.04	1.9±0.2	14.4	0.58	0.38	70	5.03	22.8
9	2.05±0.04		13.7	0.65	0.35	60	6.81	20.3
8	2.47±0.06	2.4±0.2	13.0	0.72	0.32	50	9.13	18.3

[a]k_a is the rate constant of the SCRP decay. It was measured in the laser flash ($\lambda = 308$ nm) photolysis experiments.
[b]From the best fit of TREPR spectra. Note that in this case, the values of L are slightly larger than those used in simulations of the TREPR spectra of SCRPs generated in photolysis of MDB and DMDB. This is the most likely to be a consequence of the fact that the SCRP in the case of TMDPO is more hydrophilic.
[c]Calculated from the parameters used for simulation.
[d]Other parameters used in calculations: $J_0 = -4.4\times10^{10}$ rad/s, $\lambda = 0.04$ nm, $A = 38.5$ mT, $g_a = 2.0034$ (a – diphenylphosphonyl), $g_b = 2.0006$ (b – 2,4,6, trimethylbenzoyl); and η is the TM polarization $\eta = (\rho_{T_+T_+} - \rho_{T_-T_-})/(\rho_{T_+T_+} + \rho_{T_-T_{-+}})$; $\omega_0 = 9.766979$ GHz, $\omega_1 = 10^6$ rad/s, T_{2a} =40 ns, $T_{1b} = 1$ μs, T_{2b} =160 ns, $k_s\tau = 0.58$, $k_d = 10^6$ s^{-1}, and $R = 0.75$ nm.

Table 4. Observed APS splittings and Δ_{APS}, and decay constants k_{obs}, and the sets of parameters used to simulate time-resolved ESR for the pair of diphenylphosphonyl/2,4,6-trimethylbenzoyl radicals in C_n alkyl sulfate micelles[d].

[H_2O]/[AOT]	Water core radius (Å)	J_0 (GHz)	D ($\times 10^6$ cm^2/s)	T_2 (μs)	Z ($\times 10^{-6}$ s^{-1})	$\frac{qR^2}{D}$
37	53	−3.1	2.4	0.36	5.2	0.32
	43	−3.1	1.6	0.28	8.0	0.49
23	33	−3.1	1.2	0.24	16	0.65
16	23	−3.1	0.4	0.24	30	2.0
12	17	−3.1	0.05	0.12	27	16

[a]Other parameters: g-factors of the radicals **1** and **2** respectively: $g_1 = 2.0029$, $g_2 = 2.0041$. HFI constants in radical **1**: $A_1(CH_2) = 1.91$ mT, $A_2(CH_2) = 0.422$ mT, and $A(N) = 0.22$ mT; in radical **2**: $A_1(H) = 0.121$ mT, $A_2(H) = 0.042$ mT, and $A_3(H) = 0.036$ mT; rate constant of spin-non-selective decay of radical **1** $k_1 = 1.2 \times 10^6$ s^{-1}; the probability of the singlet contact radical pair decay 0.52 was held as independent on the micelle size, maximum of the time-window function was located at 500 ns.

Table 5. Parameters used in the microreactor model simulation and the frequencies of radical encounters extracted from simulations for **Figure 11**[a].

nanoscopic cavity, that is, to integrate Eqs. (4)–(6). In such a way, we are free from the restrictions imposed by the demands of a spherical shape for the microreactor, and we can also relax the requirement of fixing one of the radical partners in the center of microreactor.

The space evolution of a pair can be explicitly calculated (**Figure 13**) in the form of trajectories $\Omega(\mathbf{s}(t))$, where $\mathbf{s}(t)$ stands for space stochastic variables limited by the demand that particles cannot penetrate into each other and cannot escape from the cavity. Instead, they can decay through a spin-selective chemical reaction with a rate constant that depends on the distance between the radicals. Then, the propagation of the spin density operator $\hat{\rho}_{\Omega}(t)$ of SCRP is given by the formal solution of Eqs. (4)–(6) under condition that the interval Δt is so small that all the parameters of SLE can be considered as time independent for this time interval:

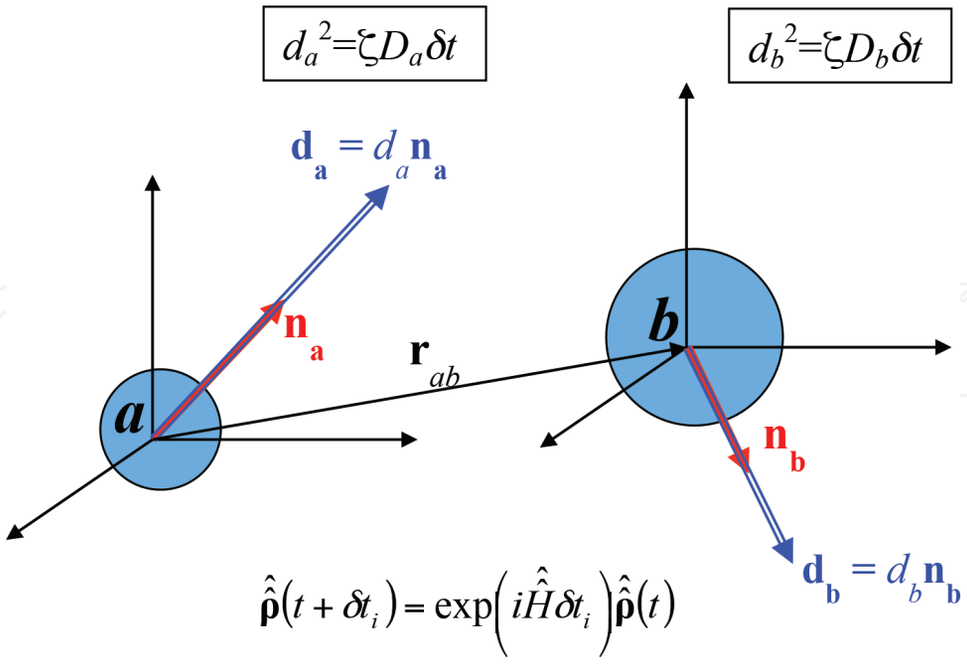

Figure 13. Random walk calculations: Each radical ***a*** and ***b*** take walks along random directions $\mathbf{n_a}$ and $\mathbf{n_b}$, ζ is the coefficient (=6 for the 3- and = 4 for the 2-dimension) depending on the dimensionality of walk. If, say, radical ***a*** attempts to penetrate into the sphere (= r_b) representing radical ***b***, then it will return to its initial position and this pair will be considered as a reacting pair according to the rules for spin-selective reaction decay. Similarly, if radical ***a*** or ***b*** attempts to cross the boundary, it will return to the starting point as well. During the time interval δt, the spin dynamics of the pair is governed by the pair spin Hamiltonian, Eq. (4), depending on the distance between the radicals r_{ab}.

$$\hat{\rho}_{\Omega}(t+\Delta t) = \exp\left\{\left(-i\hat{H}\left(\Omega(t)\right) - \hat{K}\left(\Omega(t)\right)\right)\Delta t\right\} \times \hat{\rho}_{\Omega}(t)$$
$$\times \exp\left\{\left(+i\hat{H}\left(\Omega(t)\right) - \hat{K}\left(\Omega(t)\right)\right)\Delta t\right\} \quad (12)$$

It is clear that the number of trajectories needs to be large, and the time intervals Δt should be small enough such that $|\Delta J| = |J(t+\Delta t) - J(t)| \ll |q|$. Control over the implementation of this inequality greatly accelerates the speed of our calculations [99]. We use the "crude force" method (or a capture-probability based algorithm) to investigate the steady state conditions and the kinetics of approaching it. Such a choice is dictated by that under conditions of spin–selectivity of reaction application of advanced algorithms, [100] is rather difficult. An essential drawback of the method is the practical impossibility to check convergence of the solution.

7.1. The concept of the filled-out micelle and enforced encounters

Immediately after birth at $t = 0$, the radicals of the SCRP are assumed to be at the distance of the closest approach R which can be estimated as 5–10 Å (in our calculations we always use $R = 6$ Å, except in the case of TMDPO, where $R = 7.5$ Å). Then, until one of the radicals arrives for the first time at the boundary of micelle, the radicals diffuse in such a way if they were free, that is, unrestricted by micellar containment. After this moment, it is quite reasonable to utilize, as the first approximation, the frequency Z of encounters of the SCRP partners confined in a micellar

http://dx.doi.org/10.5772/67463

phase. The parameter Z is assumed to be independent of time and space coordinates. From the kinetic point of view, the "correctness" of this intuitive approximation is warranted by the fact that any diffusing particle enclosed in an arbitrary cavity with inert walls evolves in time to a state where the probability to find a particle at any arbitrary point inside of a cavity does not depend on the coordinates of the particle. We call this the "filling out" of the cavity.

After the cavity has been filled, bimolecular reactions between two reactive particles enclosed in the cavity become monoexponential. In other words, a system comprised of two radicals approaches a steady state, provided by the reflection of diffusing radicals from the boundary back to the inside of the cavity. To distinguish this type of encounter from repetitive encounters in homogeneous media, we call them "enforced encounters." To illustrate this intuitive picture in more detail, we performed the RW calculations presented in **Figure 14**.

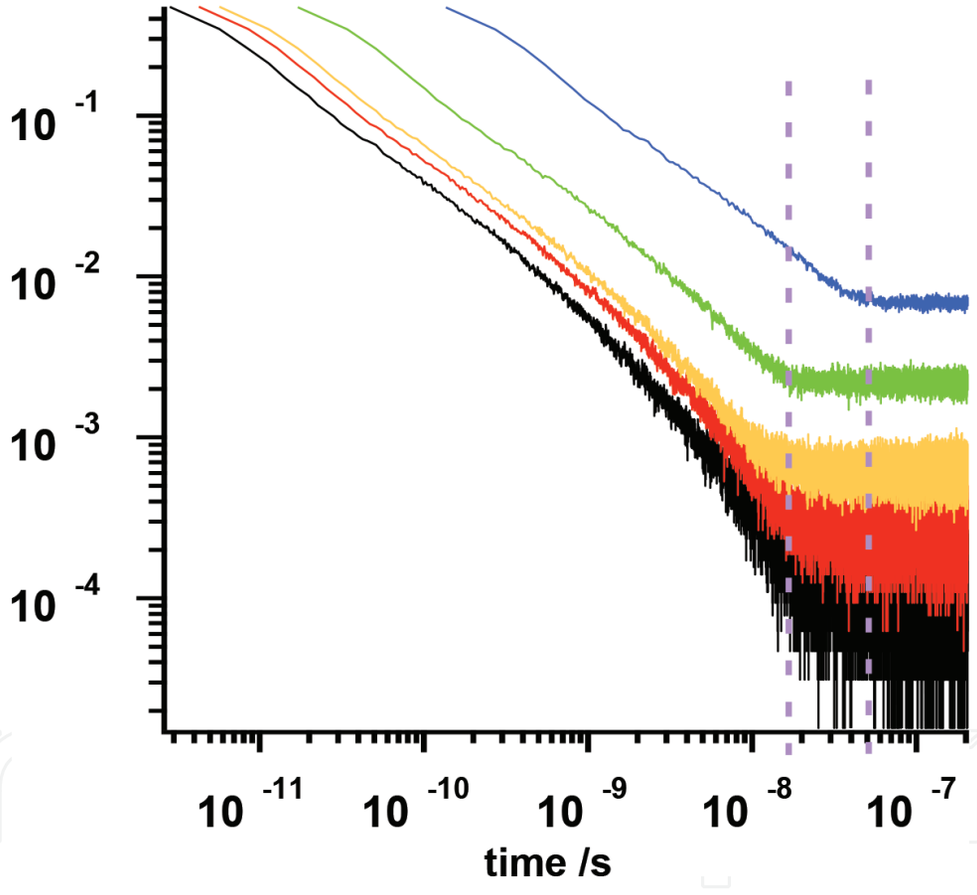

Figure 14. Filling out of AOT reverse micelles. $Lm = 53$, 33, 23, and 17×10^{-8} cm respectively for A, B, C and D traces. For the other parameters used, see section 5.4. Vertical dashed lines indicate the time of a system to arrive at the state of filled out micelle.

The probability that the next walk will be an encounter of the SCRP is shown in the plot as a function of time. Unlike our microreactor calculations, in the RW, both radicals are allowed to diffuse. In this particular calculation, the diffusion coefficients of the radicals were assumed to be the same $D_a = D_b = D$ with D taken from **Table 5**. Also, in these calculations, we propose that the SCRP is born in the center of the AOT water pool. This allows for a more direct

comparison between the RW and microreactor models. From **Figure 14**, we see that indeed initially the radicals of the SCRP diffuse as if they were in unrestricted space, and the probability of their encounters decreases with time in a $t^{-3/2}$ dependence, which is a characteristic feature of unrestricted diffusion in homogeneous media. However, at some characteristic time, the kinetic behavior of the system changes dramatically: The probability of encounter stops to depend on time. The number of random walks N_L to get the boundary is equal to *ca*. $(L_m/d)^2$ where $d = 0.64 \times 10^{-8}$ cm is the length of random walk. The time at which of one of the radicals arrives at the boundary is then $t_L = (d^2/6D) \times N_L$. The time interval for these events is shown by vertical dashed lines in the figure. Thus, at the moment of the GG-AQDS radical pair observation ($\tau_w = 500$ ns), all of the reverse micelles are filled out, and the probability of encounters no longer depends on the time after SCRP creation. A consequence of this is that the observation of ST_0RPM polarization in the case of large ($L_n = 53 \times 10^{-8}$ cm) micelles, and its total absence in the small ones ($L_n = 23 \times 10^{-8}$ and 17×10^{-8} cm) is not related to the attainment of steady state conditions.

7.2. Self-quenching of the ST_0RPM CIDEP

In **Figure 15**, we present the RW calculations of the time evolution of the ST_0RPM polarization in SCRPs resulting from photoprocesses in the GG-AQDS system described in Section 4.3.5. All the parameters (except for TM polarization, which is neglected for this case) used in the calculations are given in **Table 5**. To estimate the magnitude of polarization, we calculated the population differences, being initially of zero value, between the $|\alpha\beta>$ and $|\beta\alpha>$ electron spin states of a pair with representative value 24 G for the hyperfine coupling constant (**Table 5**).

In the smallest micelles ($L_m = 17$ Å), the lifetime $\tau_D = R^2/D$ of the primary solvent cage equals 80 ns. **Figure 15** shows (black line) that strong ST_0RPM polarization has been created, but it is

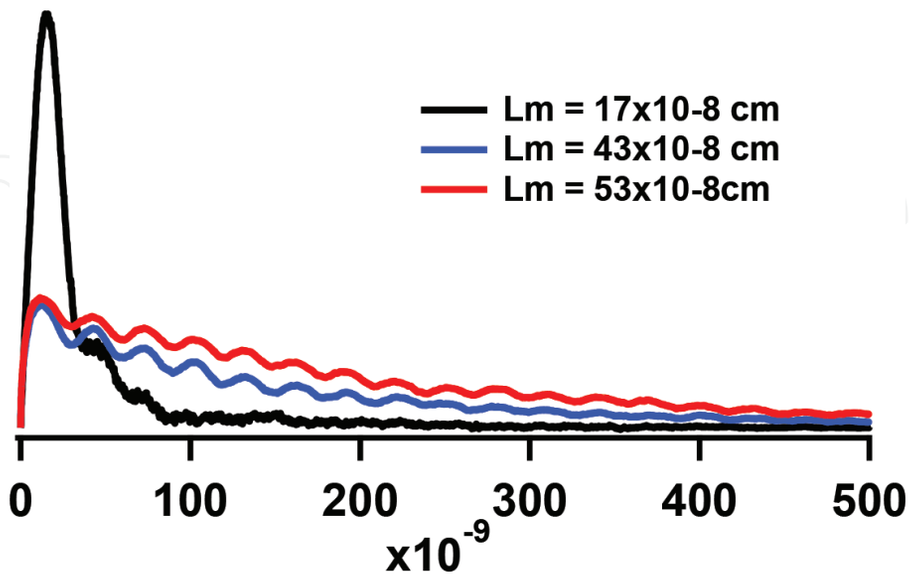

Figure 15. Generation and decay over time of the ST_0RPM polarization in AOT reverse micelles. Water core radii are given in the insertion. All other parameters are listed in **Table 4**. The TM polarization is neglected.

http://dx.doi.org/10.5772/67463

quenched during the lifetime of the primary solvent cage. This well agrees with the theoretical prediction [101] that if the geminate life is too long that $q\tau_D$ (=34) ≫ 1, then ST_0RPM polarization cannot be created. This is because the phase of the SCRP spin function becomes randomized during the encounter. In large micelles (L_m = 43 Å and 53 Å), the radicals escape the primary geminate cage being ST_0RPM polarized (blue and red lines). Thus, the RW calculations presented in **Figure 15** clearly demonstrate that it is not that the APS is transformed into the ST_0RPM but rather that the ST_0RPM polarization is created first and then is converted into the APS pattern. A question that can be asked is why the ST_0RPM polarization decreases after that

The resonance frequencies in the spin system of the SCRP are modulated by electron spin-spin Heisenberg exchange through the $\omega \pm J$ and $\pm\varepsilon$ terms (see Eq. (8) in **Table 1**). The first of these processes causes flip-flop electron spin transitions $|\alpha\beta;\chi\rangle \leftrightarrow |\beta\alpha;\chi\rangle$ which leads to annealing of the populations of corresponding spin states. The second process provides so-called "dephasing," because it splits the rotation of transverse magnetization of the RP into two components [81] and prevents the generation of ST_0RPM polarization in subsequent encounters. **Figure 16** illustrates the decay of ST_0RPM polarization due to enforced encounters. The initial state of a pair is the $|\alpha\beta\rangle$ spin state. Due to forced encounters, the exchange interaction induces flip-flop transitions in the contact pairs thereby generating a population of the $|\beta\alpha\rangle$ spin state. As follows from **Figure 16**, the system approaches to the state without any stationary polarization. Thus, the ST_0RPM polarization observed in escaped radicals is just nothing but the remnants of non-extinguished ST_0RPM polarization generated at the initial stage of SCRP life in a closed volume formed by heterogeneity, the size of which is on the nanometer scale.

We have demonstrated that the TREPR spectroscopy of SCRPs can be an effective and extremely informative tool to investigate molecular dynamics in inhomogeneous structures on the nanometer scale. The spectral shape of the APS (its components and values of spectral shifts), the contributions from ST_0RP and/or ST_RPM polarization, together with the TM

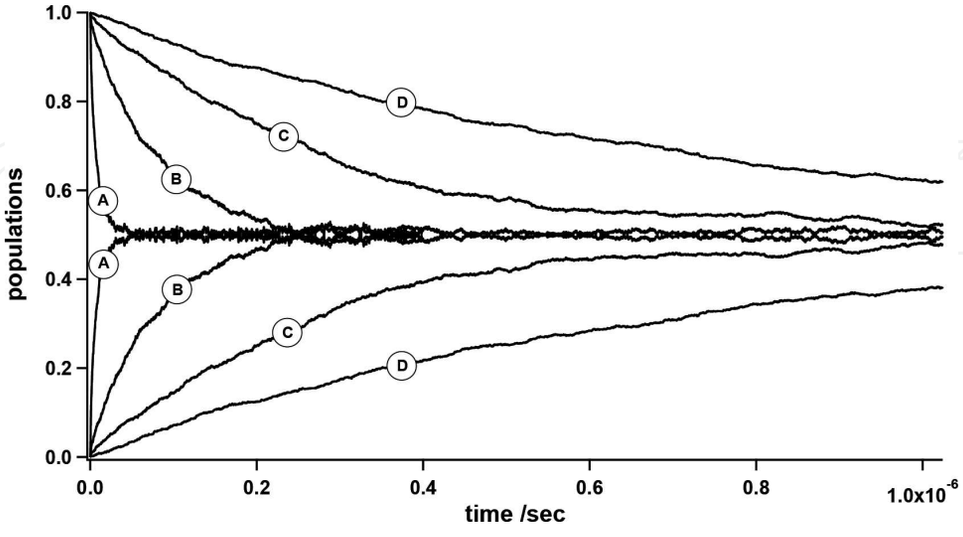

Figure 16. Relaxation of populations due to electron spin–spin exchange interaction as function of micelle size. L_m = 16 Å (A), 32 Å (B), 48 Å (C), and 64 Å (D). Both radicals diffuse, no escape, no chemical reaction, $J_0 = -2\times10^{10}$ rad/s; λ = 0.5 Å; $D_a = D_b = 10^{-6}$ cm^2.

polarization and regular encounters with rates depending on the sizes and shapes of the inhomogeneous structure provide extremely rich material for discussion, modeling, and experimentation.

The nature of the information supplied by polarized spin probes is by no means local. Rather, it is a kind of average over the volume of inhomogeneity. Through observation and simulation of the APS, we first of all demonstrate that there is no such a thing as a "location" of radicals inside inhomogeneity. If radicals were in fixed locations, then their TREPR spectra would look very different from those shown in **Figures 4**, **5**, and **8**–**12**.

Author details

Valery F. Tarasov[1] and Malcolm D.E. Forbes[2]*

*Address all correspondence to: forbesm@bgsu.edu

1 Semenov Institute of Chemical Physics, Moscow, Russia

2 Center for Photochemical Sciences, Department of Chemistry, Bowling Green State University, Bowling Green, Ohio, USA

References

[1] A.F. Vanin, N.A. Sanina, V.A. Serezhenkov, D.Sh. Burbaev, V.I. Losynsky, S.N. Aldoshin. Dinitrosyl–iron complexes with thiol–containing ligands: Spatial and electronic structures. Nitric Oxide Biol. Chem. **16** (2007) 62–93.

[2] G.I. Likhtenshtein "Nitroxide Spin Probes for Studies of Molecular Dynamics and Microstructure" Chapter 6, p. 205 in G.I. Likhtenshtein, J. Yamauchi, S. Nakatsuji, A. Smirnov, R. Tamura (Eds) Nitroxides: Applications in chemistry, biochemistry and materials science. Wiley – VCH Verlag GmbH & Co.KGaA (2008).

[3] A.I. Kokorin (Ed). *Nitroxides – Theory, experiment and applications.* Croatia (2012), 436 p. A free online edition of this book is available at www.intechopen.com

[4] B.H. Robinson, H. Thomann, A.H. Beth, P. Fajer, L.R. Dalton. The phenomenon of magnetic resonance: Theoretical considerations. In EPR and Advanced EPR Studies of Biological Systems. L.R. Dalton (Ed.). C.R.C.Press Boca Raton FL 1 – 314.

[5] A.L. Buchachenko, A.M. Wasserman. *Stable radicals*. Khimiya, Moscow (1979), p. 410.

[6] D.E. Budil, S. Lee, S. Saxena, J.H. Freed. Nonlinear–least–squares analysis of slow–motion EPR spectra in one and two dimensions using a modified Levenberg–Marquardt algorithm. J. Magn. Reson. A **120** (1996) 155–189.

[7] S. Stoll, A. Schweiger. EasySpin, a comprehensive software package for spectral simulation and analysis in EPR. J. Magn. Reson. **178** (2006) 42–55.

[8] F.H. Cho, V. Stepanov, S. Takahashi. A high-frequency electron paramagnetic resonance spectrometer for multi-dimensional, multi-frequency, and multi-phase pulsed measurements. Rev. Sci. Instrum. **85** (2014) 075110.

[9] A.J. Hoff (Ed). *Advanced EPR. Application in biology and biochemistry*. Elseiver Science Publishers B.V., Amsterdam, Oxford, New York and Tokyo (1989), 918 p.

[10] S.A. Dikanov, Yu D. Tsvetkov. *Electron spin echo envelope modulation (ESEEM) spectroscopy*. CRC Press, Boca Raton, Ann Arbor, London and Tokyo (1992), 412 p.

[11] L.J. Berliner, S.S. Eaton, G.R. Eaton (Eds). *Biological magnetic resonance. Distance measurements in biological systems by EPR*, Vol. 19. Kluwer Academic Publishers, New York, Boston, Dordrecht, London and Moscow (2002), p. 614.

[12] J. B. Feix and C. S. Klug "Site–Directed spin labeling of membrane proteins and peptide–membrane interactions" in L.J. Berliner (Ed) "Biological Magnetic Resonance, Spin Labeling: The Next Millennium, 14, Plenum Press, New York (1998) pp. 251 – 281

[13] Yu E. Nesmelov, D.D. Thomas. Protein structural dynamics revealed by site–directed spin labeling and multifrequency EPR. Biophys. Rev. **2** (2010) 91–99.

[14] D. Marsh. Spin–label EPR for determining polarity and proticity in biomolecular assemblies: Transmembrane profiles. Appl. Magn. Reson. **37** (2010) 435–454.

[15] C.F. Polnaszek, J.H. Freed. Electron spin resonance studies of anisotropic ordering, spin relaxation and slow tumbling in liquid crystalline solvents. J. Phys. Chem. **79**:2 (1975) 2283–2306.

[16] P.J. Wagner, G.S. Hammond. In A.W. Noyes, G.S. Hammond, J.N. Pitts (Eds) *Advances in photochemistry*. Wiley, Hoboken, NJ (2007), p. 5.

[17] W.M. Haynes. *CRC handbook of chemistry and physics* (94th ed.). CRC Press, Boca Raton, FL (2013).

[18] R.W. Fessenden, R.H. Schuler. Electron spin resonance studies of transient alkyl radicals. J. Chem. Phys. **39**:9 (1963) 2147–2195.

[19] J. Bargon. The discovery of chemically induced dynamic polarization (CIDNP). Helv. Chim. Acta **89** (2006) 2082–2102.

[20] H.R. Ward, R.G. Lawler. Nuclear magnetic resonance emission and enhanced absorption in rapid organometallic reactions. J. Am. Chem. Soc. **89** (1967) 5518–5519.

[21] E. Wigner, E.E. Witner. On the structure of the spectra of two–atomic molecules according to quantum mechanics. Z. Phys. **51** (1928) 859. In H. Hetema (Ed) *Quantum chemistry: Classic scientific papers.* World Scientific, Singapore, New Jersey, London and Hog Kong (2000), pp. 287–311.

[22] K.M. Salikhov, Yu N. Molin, R.Z. Sagdeev, A.L. Buchachenko. *Spin polarization and magnetic effects in radical reactions*. Akadémiai Kiadó, Budapest (1984), p. 419.

[23] H. Hayashi. *Introduction to dynamic spin chemistry. Magnetic field effects on chemical and biochemical reactions*. World Scientific Lecture and Course Notes in Chemistry, Vol. 8. S. H. Lin Editor-in-charge. World Scientific (2004).

[24] G.L. Closs. Chemically induced dynamic nuclear polarization. Adv. Magn. Reson. **7** (1974) 157–229.

[25] R. Kaptein. Chemically induced dynamic nuclear polarization: Theory and applications in mechanistic chemistry. Adv. Free Radic. Chem. **5** (1975) 319–380.

[26] U.E. Steiner, T. Ulrich. Magnetic field effects in chemical kinetics and related phenomena. Chem. Rev. **89**:1 (1989) 51–147.

[27] F.S. Sarvarov, K.M. Salikhov. Theory of spin–dependent recombination of radicals in homogeneous solution. React. Kinet. Catal. Lett. **4** (1976) 33–41.

[28] J.B. Pedersen. High field CIDNP. General analytic results. J. Chem. Phys. **67**:9 (1977) 4097–4102.

[29] L. Monchick, F.J. Adrian. On the theory of chemically induced electron polarization (CIDEP): Vector model and an asymptotic solution. J. Chem. Phys. **68** (1978) 4376–4383.

[30] F.J. Adrian. Theoretical aspects of chemically induced magnetic polarizations. Res. Chem. Intermed. **16** (1991) 99–125.

[31] J.B. Pedersen, J.H. Freed. Theory of chemically induced dynamic electron polarization. I. J. Chem. Phys. **58** (1973) 2746–2762.

[32] J.B. Pedersen, J.H. Freed. Theory of chemically induced dynamic electron polarization. II. J. Chem. Phys. **59** (1973) 2869–2885.

[33] J.B. Pedersen, J.H. Freed. Theory of chemically induced dynamic electron polarization. III. Initial triplet polarization. J. Chem. Phys. **62** (1975) 1706–1711.

[34] P.W. Atkins, G.T. Evans. Electron spin polarization in a rotating triplet. Mol. Phys. **27** (1974) 1633–1644.

[35] I.S.M. Saiful, J.–I. Fujisawa, N. Kobayashi, Y. Ohba, S. Yamauchi. A study of electron spin polarization transfer in a system of photo–excited phthalocyanine and a nitroxide radical. Bull. Chem. Soc. Jpn. **72** (1999) 661–667.

[36] M.T. Colvin, R. Carmieli, T. Miura, S. Richert, D.M. Gardner, A.L. Smeig, S.M. Dyar, S. M. Conron, M.A. Ratner, M.R. Wasielewski. Electron spin polarization transfer from photogenerated spin–correlated radical pairs to a stable radical observer spin. J. Phys. Chem. A **117** (2013) 5314–5325.

[37] S. Yamauchi. Recent developments in studies of electronic excited states by means of electron paramagnetic resonance spectroscopy. Bull. Chem. Soc. Jpn. **77** (2004) 1255–1268.

[38] A.I. Shushin. Diffusion theory of CIDEP spectra of spin correlated radical pairs. Chem. Phys. Lett. **177** (1991) 338–344.

[39] G.L. Closs, M.D.E. Forbes, J.R. Norris, Jr. Spin–polarized electron paramagnetic resonance spectra of radical pairs in micelles. Observation of electron spin–spin interactions. J. Phys. Chem. **91**:13 (1987) 3592–3599.

[40] V.R. Gorelik, V.F. Tarasov, S.R. Shakirov, E.G. Bagryanskaya. Effect of nitroxide radicals on chemically induced dynamic electron polarization of spin–correlated radical pairs in aqueous micellar solutions of sodium dodecy sulfate. Russ. Chem. Bull. Int. Ed. **57**:7 (2008) 1416–1427.

[41] A.L. Konkin, H.–K. Roth, M. Schroedner, G.A. Nazmutdinova, A.V. Aganov, T. Ida, R.R. Garipov. Time-resolved EPR study of radicals from 2,2-dimethoxy-2-phenylacetophenone in ethylene glycol after flash photolysis. Chem. Phys. **287** (2003) 377–389.

[42] A.N. Savitsky, H. Paul. Quantitative time-resolved EPR CIDEP study of the photodecomposition of *trans*-azocumene in solution. Appl. Magn. Reson. **12** (1997) 449–464.

[43] K. Hasharoni, H. Levanon, M.K. Bowman, J.R. Norris, D. Gust, T.A. Moore, A.L. Moore. Analysis of time-resolved CW_EPR spectra of short-lived radicals at different times after laser excitation. Appl. Magn. Reson. **1** (1990) 357–368.

[44] A.G. Redfield. Nuclear magnetic resonance and rotary saturation in solids. Phys. Rev. **98** (1955) 1787–1809.

[45] T.N. Makarov, H. Paul. Analysis of EPR-time profiles of transient radicals with unresolved spectra. J. Magn. Reson. **169** (2004) 335–341.

[46] V.F. Tarasov, I.S.M. Saiful, Y. Iwasaki, Y. Ohba, A. Savitsky, K. Mobius, S. Yamauchi. Electron spin polarization in an excited triplet-radical pair system: Generation and decay of the state. Appl. Magn. Reson. **30** (2006) 619–636.

[47] N.J. Turro, M.H. Kleinman, E. Karatekin. Electron spin polarization and time–resolved electron paramagnetic resonance: Applications to the paradigms of molecular and supramolecular photochemistry. Angew. Chem. Int. Ed. **39** (2000) 4436–4461.

[48] G. Kroll, M. Pluschau, K.-P. Dinse, H. van Willigen. Fourier transform–electron paramagnetic resonance spectroscopy of correlated radical pairs. J. Chem. Phys. **93**:12 (1990) 8709–8716.

[49] C.M.R. Clancy, V.F. Tarasov, M.D.E. Forbes. Time–resolved electron paramagnetic resonance studies in organic photochemistry. In B.C. Gilbert, N.M. Atherton, M.J. Davies (Eds) *Electron paramagnetic resonance, specialist periodical reports*, Vol. 16. Royal Society of Chemistry, Cambridge, UK, (1998), pp. 50–78.

[50] M.D.E. Forbes, L.E. Jaroha, S.Y. Sim, V.F. Tarasov. Time resolved spectroscopy: History, technique, and application to supramolecular and macromolecular chemistry. Adv. Phys. Org. Chem. **47** (2013) 1–83.

[51] M. Goez. An introduction to chemically induced dynamic nuclear polarization. Concepts Magn. Reson. **7** (1995) 69–86.

[52] E. Davidso, G. Jeschke, G. Matysik. Photo–CIDNP MAS NMR. In T.J. Aaartsma, J. Matysic (Eds) *Biophysical techniques in photosysnthesis II*. Springer, Dordrecht, The Netherlands (2008), pp. 385–399.

[53] K.H. Mok, P.J. Hore. Photo–CIDNP NMR methods studying protein folding. Methods **34** (2004) 75–87.

[54] E.G. Bagranskaya, R.Z. Sagdeev. Dynamic and stimulated nuclear polarization in photochemical radical reactions. Russ. Chem. Rev. **69** (2000) 925–945.

[55] K.A. McLauchlan, S.R. Nattrass. Experimantal studies of the spin–correlated radical pair in micellar and microemulsion media; MARY, RYDMR B_0 and RYDMR B_1 spectra. Mol. Phys. **65** (1988) 1483–1503.

[56] S.N. Batchelor, K.A. McLauchlan, I.A. Shkrob. Reaction yield detected magnetic resonance and magnetic field effect studies of radical pairs containing electronically excited organic radicals. Mol. Phys. **77** (1992) 75–109.

[57] J.R. Woodward, C.R. Timmel, P.J. Hore, K.A. McLauchlan. Low field RYDMR: Effects of orthogonal static and oscillating magnetic fields on radical recombination reactions. Mol. Phys. **100** (2002) 1181–1186.

[58] S. Aich, S. Basu. Magnetic field effect: A tool for identification of spin state in a photoinduced electron–transfer reaction. J. Phys. Chem. A **102** (1998) 722–729.

[59] K. Schulten. Magnetic field effects in chemistry and biology. In J. Treusch (Ed) *Festrorperperproblem.* Advances in solid state physics, Vol. XXII. Vieweg, Braunschweig (1982), pp. 61–83.

[60] C.B. Grisom. Magnetic field effects in biology: A survey of possible mechanisms with emphasis on radical–pair recombination. Chem. Rev. **95** (1995) 3–24.

[61] V.F. Tarasov, N.D. Ghatlia, N.I. Avdievich, I.A. Shkrob, A.L. Buchachenko, N.J. Turro. Examination of the exchange interaction through micelle size. 2. Isotope separation efficiency as an experimental probe. J. Am. Chem. Soc. **116** (1994) 2281–2291.

[62] A.L. Buchachenko. Magnetic isotope effect: Nuclear spin control of chemical reactions. J. Phys. Chem. A **105** (2001) 9995–10011.

[63] A.R.P. Rau. Manipulating two–spin coherences and qubit pairs. Phys. Rev. A **61** (2000) 032301.

[64] X. Hu, S.D. Sarma. Hilbert–space structure of a solid–state quantum computer: Two electron states of a double–quantum–dot artificial molecule. Phys. Rev. A **61** (2000) 062301.

[65] Y. Omar, N. Paunkovic, S. Bose, V. Vedral. Spin–space entanglement transfer and quantum statistics. arXiv:quant–ph/0105120 **2** (2002) 5.

[66] D.P. DiVincenzo. Real and realistic quantum computers. Nature **393** (1998) 113–114.

[67] S.D. Sarma. Spintronics. A new class of device based on electron spin, rather than on charge, may yield the next generation of microelectronics. Am. Sci. **89** (2001) 516–523.

[68] C.D. Buckley, D.A. Hunter, P.J. Hore, K.A. McLauchlan. Electron spin resonance of spin–correlated radical pairs. Chem. Phys. Lett. **135** (1987) 307–311.

[69] Y. Sakaguchi, H. Hayashi, H. Murai, Y.J. I'Haya. CIDEP study of the photochemical reactions of carbonyl compounds showing the external magnetic field effect in a micelle. Chem. Phys. Lett. **110** (1984) 275–279.

[70] Y. Sakaguchi, H. Hayashi, H. Murai, Y.J. I'Haya, K. Mochida. CIDEP study of the formation of a cyclohexadienyl–type radical in the hydrogen abstraction reactions of triplet xanthone. Chem. Phys. Lett. **120** (1985) 401–405.

[71] H. Murai, Y. Sakaguchi, H. Hayashi, Y.J. I'Haya. An anomalous phase effect in the individual hyperfine lines of the CIDEP spectra observed in the photochemical reactions of benzophenone in micelles. J. Phys. Chem. **90** (1986) 113–118.

[72] A.D. Trifunac, D.J. Nelsen. Chemically induced dynamic electron polarization. Pulse radiolysis of aqueous solutions of micelles. Chem. Phys. Lett. **46** (1977) 346–348.

[73] G.L. Closs, M.D.E. Forbes, J.R. Norris, Jr. Spin–polarized electron paramagnetic resonance spectra of radical pairs in micelles. Observation of electron spin–spin interactions. J. Phys. Chem. **91** (1987) 3592–3599.

[74] S.H. Glarum, J.H. Marshall. Spin exchange in nitroxide biradicals. J. Chem. Phys. **47** (1967) 1374–1378.

[75] H. Yonemura, M.D.E. Forbes. Electron spin exchange in linked phenothiazine–viologen charge transfer complexes incorporated in "through–ring" (rotaxane) α–cyclodextrins. Photochem Photobiol. **91** (2015) 672–677.

[76] P. Caregnato, L.E. Jarocha, H.S. Esinhart, N.V. Lebedeva, V.F. Tarasov, M.D.E. Forbes. Electrostatic control of spin exchange between mobile spin–correlated radical pairs created in micellar solutions. Langmuir **112** (2011) 7574–7580.

[77] A. Kawai, A. Shikama, M. Mutsui, K. Obi. Time resolved ESR study on the photochemical reactions of pyrene and nitroxide radical system in micelle; formation of spin–correlated pyrene cation – nitroxide pairs. Bull. Chem. Soc. Jpn. **74** (2001) 1203–1211.

[78] E.E. Chaney, M.D.E. Forbes. Dynamics of spin–correlated radical pairs in non–ionic surfactant solutions. J. Phys. Chem. B **107** (2003) 4464–4469.

[79] S. Moribe, T. Ikoma, K. Akiyama, S. Tero–Kubota. Time–resolved EPR study on photoreduction of sodium anthraquinone–2–sulfate in liposome. Chem. Phys. Lett. **457** (2008) 66–68.

[80] Q. Mi, M.A. Ratner, M.R. Wasielewski. Time–resolved EPR spectra of spin–correlated radical pairs: Spectral and kinetic modulation resulting from electron–nuclear hyperfine interactions. J. Phys. Chem. A **114** (2010) 162–171.

[81] V.F. Tarasov, M.D.E. Forbes. Time resolved electron spin resonance of spin correlated micelle confined radical pairs. Shape of the anti–phase structure. Spectrochim. Acta A **56** (2000) 245–263.

[82] V.F. Tarasov, L.E. Jarocha, N.I. Avdievich, M.D. Forbes. TREPR spectra of micelle – confined spin correlated radical pairs. I. Molecular motion and simulations. Photochem. Photobiol. Sci. **13** (2014) 439–453.

[83] C.–H. Wu, W.S. Jenks, I.V. Koptyug, N.D. Ghatlia, M. Lipson, V.F. Tarasov, N.J. Turro. Time–resolved ESR examination of a simple supramolecular guest–host system. Electron spin exchange interaction in micellized spin–correlated radical pairs. J. Am. Chem. Soc. **115** (1993) 9583–9595.

[84] V.F. Tarasov, H. Yashiro, K. Maeda, T. Azumi, I.A. Shkrob. Spin–correlated radical pairs in micellar systems: Mechanism of CIDEP and the micelle size dependence. Chem. Phys. **212** (1996) 353–361.

[85] V.F. Tarasov, H. Yashiro, K. Maeda, T. Azumi, I.A. Shkrob. Time–resolved ESR in a spin–correlated radical pair with large hyperfine coupling constant at ^{31}P. Micellar size effects and the role of flip–flop transitions. Chem. Phys. **226** (1998) 253–269.

[86] K. Maeda, M. Terazima, T. Azumi, Y. Tanimoto. CIDNP and CIDEP studies on intramolecular hydrogen abstraction reaction of polymethylene–linked xanthone and xanthene. Determination of the exchange integral of the intermediate biradicals. J. Phys. Chem. **95** (1991) 197–204.

[87] K. Tominaga, S. Yamauchi and N. Hirota. A chemically induced dynamic electron polarization study on the acetone ketyl radical and radical pair in an alcohol solution. J. Chem. Phys. **92** (1990) 5175–5185.

[88] A.I. Shushin. The cage effect and ESR spectra of spin–correlated radical pairs. Chem. Phys. Lett. **162** (1989) 409–415.

[89] L. Sterna, D. Ronis, S. Wolfe, A. Pines. Viscosity and temperature dependence of the magnetic isotope effect. J. Chem. Phys. **73**:11 (1980) 5493–5499.

[90] V.F. Tarasov, A.L. Buchachenko, V.I. Maltsev. Magnetic isotope effect and isotope separation in microreactors. Russ. J. Phys. Chem. **55** (1981) 1921–1928.

[91] V.F. Tarasov, N.D. Ghatlia, N.I. Avdievich, I.A. Shkrob, A.L. Buchachenko, N.J. Turro. Examination of the exchange interaction through micelle size. 2. Isotope separation efficiency as an experimental probe. J. Am. Chem. Soc. **116** (1994) 2281–2291.

[92] N.J. Turro, G.S. Cox, M.A. Paczkowski. Photochemistry in micelles. Top. Curr. Chem. **129** (1985) 57–97.

[93] M. Tachiya. Stochastic and diffusion models of reactions in micelles and vesicles. In G.R. Freeman (Ed) Kinetics of nonhomoheneous processes. A practical introduction for chemists, biologists, physicists, and materials scientists. John Wiley & Sons, Inc., New York, NY, (1987) 575–650

[94] V.F. Tarasov, N.D. Ghatlia, A.L. Buchachenko, N.J. Turro. Probing the exchange interaction through the micelle size. 1. Probability of recombination of triplet geminate radical pairs. J. Am. Chem. Soc. **114** (1992) 9517–9526.

[95] R.C. White, V.F. Tarasov, M.D.E. Forbes. Photooxidation of diglycine in confined media. Application of the microreactor model for spin–correlated radical pairs in reverse micelles and water–in–oil microemulsions. Langmuir **21** (2005) 2721–2727.

[96] V.F. Tarasov, L.E. Jaroha, M.D. Forbes. TREPR spectra of micelle – confined spin correlated radical pairs. II. Spectral decomposition and asymmetric line shapes. Photochem. Photobiol. Sci. **13**:2 (2014) 454–463.

[97] Y. Sakaguchi, H. Hayashi, H. Murai, Y.J. I'Haya. CIDEP study of the photochemical reactions of carbonyl compounds showing the external magnetic field effect in a micelle. Chem. Phys. Lett. **110** (1984) 275–279.

[98] M. Hasegawa, T. Sugimura, Y. Suzaki, Y. Suzaki, Y. Shindo. Microviscosity in water pool of aerosol–OT reversed micelle determined with viscosity–sensitive fluorescenck probe, auramine 0, and fluorescence depolarization of xanthene dyes. J. Phys. Chem. **98** (1994) 2120–2124.

[99] K.L. Aminov, J.B. Pedersen. Improved finite difference calculation of magnetic field effects: Inclusion of analytic asymptotics. Chem. Phys. **193** (1995) 297–308.

[100] H.–X. Zhou. Comparison of three Brownian–dynamics algorithms for calculating rate constants of diffusion–influenced reactions. J. Chem. Phys. **108** (1998) 8139–8145.

[101] J.H. Freed, J.B. Pedersen. Theory of chemically induced dynamic spin polarization. Adv. Magn. Reson. **8** (1976) 1–84.

IntechOpen